Water Science & Technology

Water Science & Technology Vol 88 No 5, 1207 doi: 10.2166/wst.2023.270

Removal of water pollutants using plant-based nanoscale zero-valent iron: A review

Urvashi Kheskwani and M. Mansoor Ahammed *

Department of Civil Engineering, Sardar Vallabhbhai National Institute of Technology, Surat 395007, India
*Corresponding author. E-mail: mansoorahammed@gmail.com

MMA, 0000-0002-8466-7528

ABSTRACT

Nanotechnology has been increasingly explored for the treatment of various waste streams. Among different nanoparticles, nanoscale zerovalent iron (nZVI) has been extensively investigated due to its high reactivity and strong reducing power. However, conventional methods for the synthesis of nZVI particles have several limitations and led to the green synthesis of nZVI using plant-based materials. Plant extracts contain various reducing agents that can be used for nZVI synthesis, eliminating the need for toxic chemicals, and reducing energy consumption. Additionally, each plant species used for nZVI synthesis results in unique physicochemical properties of the nanoparticles. This review paper provides an overview of plant-based nZVI particle synthesis, its characteristics, and its application for the removal of different classes of pollutants such as dyes, heavy metals, nutrients, and trace organic pollutants from water. The review shows that continued research on plant-based nZVI particles to fully understand its potential in wastewater treatment, especially for the removal of a wider variety of pollutants, and for improving sustainability and reducing the cost and environmental impact of the process, is necessary.

Key words: adsorption, dyes, green synthesis, heavy metals, plant-based nZVI, plant extracts

HIGHLIGHTS

- A variety of plants and plant parts can be used for the synthesis of nanoscale zerovalent iron particles.
- Plant-based nZVI particles show improved material characteristics.
- A variety of water contaminants can be removed using plant-based nZVI.
- Studies indicate that plant-based nZVI can be successfully regenerated.
- More studies for improving sustainability and reducing the cost of synthesis are necessary.

GRAPHICAL ABSTRACT

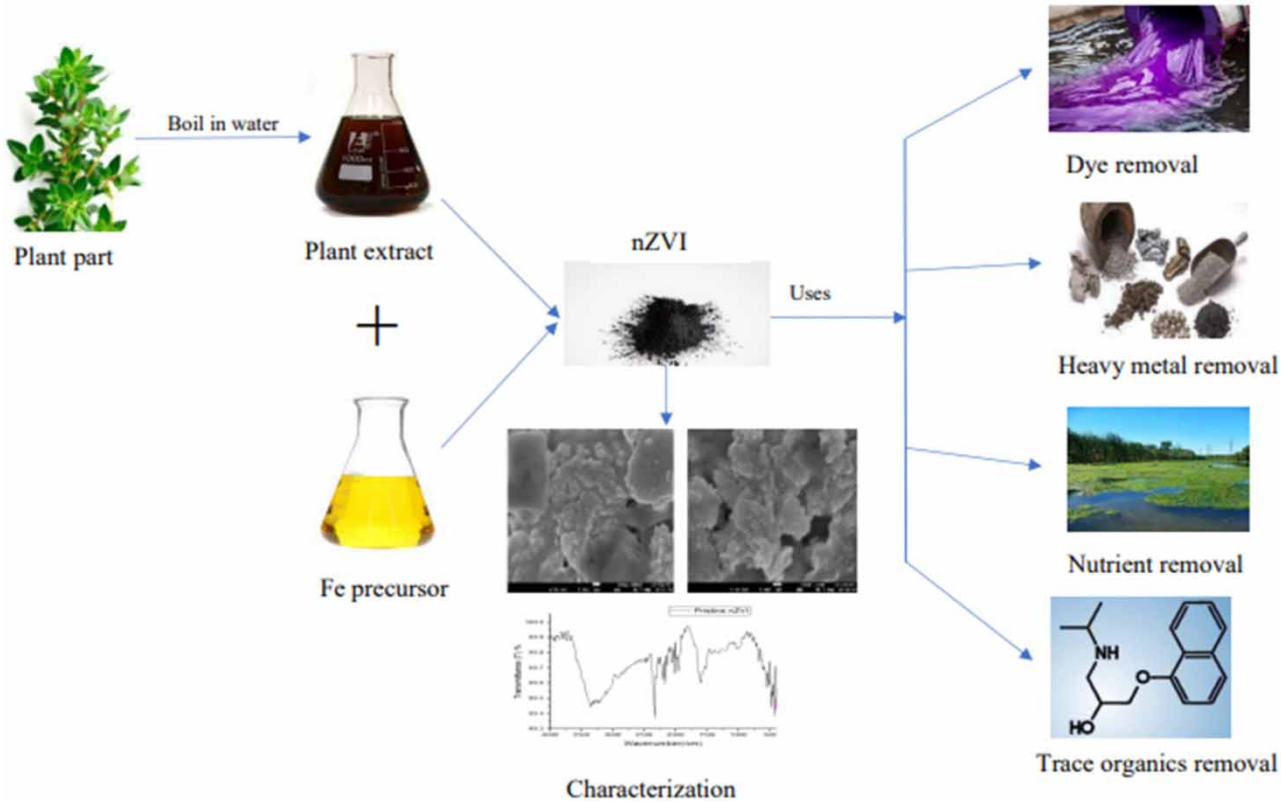

1. INTRODUCTION

In the last few decades, the use of nanotechnology for the treatment of different waste streams has increased, and nanoparticles have been widely investigated for the treatment of a variety of organic and inorganic pollutants in water/wastewater (Jamkhande *et al.* 2019). Metallic nanoparticles, because of their small size ranging between 1 and 100 nm and high reactivity, have shown high efficiency in removing different contaminants (Priya *et al.* 2021). Various metals such as gold, silver, palladium, platinum, iron, nickel, and copper have been used to synthesize nanomaterials for pollutant removal (Lu & Astruc 2020).

Among the different nanoparticles, nanoscale zerovalent iron (nZVI) is one of the most commonly investigated materials. nZVI is a magnetic material and has gained popularity due to its size, low energy requirement for synthesis, low toxicity levels, high pollutant removal efficiency, easy accessibility, and minimal secondary pollution (Zhou *et al.* 2022). It is highly regarded due to its high specific surface area which increases the number of active sites, even if a small quantity of nanoparticles is used for adsorption in the process of pollutant removal (Li *et al.* 2017a). The reducing power of nZVI in solution is strong (standard reduction potential = −0.44 V), empowering it to reduce several different kinds of contaminants such as dyes, pharmaceutical compounds, pesticides, metals, and nutrients from wastewater (Eljamal *et al.* 2020).

Nanoparticles can be synthesized using two different approaches: top-down and bottom-up. Top-down methods for nZVI production involve converting bulk particles of iron to smaller nanosized particles by milling processes, pulsed laser ablation, or noble gas sputtering, while the bottom-up approach involves aggregating smaller particles, molecule by molecule, and thus, chemically synthesizing nZVI from either dissolved iron salts, nanosized iron oxides, or iron-containing molecules, by methods such as vapor deposition method, hydrothermal method, sol-gel method, spray pyrolysis, and laser pyrolysis (Saravanan *et al.* 2021). Both these approaches have various disadvantages. The use of the top-down method generates the risk of combustion hazards and requires heavy equipment which makes the process expensive and highly energy consuming. The bottom-up approach generates toxic by-products and is expensive because of the use of high amount of chemicals as reducing agents. It requires an inert atmosphere and, hence, is done on a small scale (Pasinszki & Krebsz 2020).

At the nanoscale, it is easy for Fe^0 particles to agglomerate and get oxidized to Fe^{+2} or Fe^{+3} when exposed to air or water, thereby weakening its reducing capacity due to an increase in size (Tang *et al.* 2021). To minimize aggregation, increase stability and mobility, and reduce leaching, a wide range of inorganic and organic support and capping materials are used for nZVI (Adusei-Gyamfi & Acha 2016). These common modifications are conducted via chemical methods and involve the release of toxic by-products, the use of an expensive reducing reagent like sodium borohydride ($NaBH_4$), and high energy consumption (Yang *et al.* 2021).

Conventional methods used for the removal of water contaminants, in turn, cause other environmental problems due to the use of excessive energy and toxic chemicals (Venkatas *et al.* 2022). A sustainable solution to overcome these limitations is the green synthesis of nZVI which is economic and nontoxic, involves minimum by-product formation, and most of the time, does not require a separate capping agent, thereby reducing energy consumption and the use of toxic reducing agents (Bharti *et al.* 2021). Green materials contain polyphenols and proteins that can replace chemical reagents as reducing agents to reduce multivalent iron ions into their zerovalent states and also can act as capping agents, preventing agglomeration of particles (Mahajan *et al.* 2021). Green synthesis of nZVI can be done using microorganisms and plant extracts from flower, leaf, fruit, and stem (Ying *et al.* 2022).

Due to the limitations of maintaining the media culture and specific conditions required in the use of microorganisms, arguably the most interesting and most environmentally friendly form of green synthesis is by utilizing plant or food scraps, to create nZVI as plant extracts having various ketones, aldehydes, polyphenols, flavonoids, caffeine, and carbohydrates, making them excellent reducing agents (Huston *et al.* 2021). However, each plant used as a raw material has unique phytochemicals, and so, the nanoparticles produced have different physicochemical properties, which is an advantage of plant-mediated synthesis (Ebrahiminezhad *et al.* 2018).

Several papers recently reviewed the application of nZVI for the removal of different contaminants from water (Kalra & Gupta 2019; Li *et al.* 2021; Tarekegn *et al.* 2021). However, no review is available on the use of nZVI synthesized from plant-based materials. This paper first summarizes the synthesis of plant-based nZVI and their characteristics. Removal of different classes of pollutants such as dyes, heavy metals, nutrients, and trace organic pollutants by these nZVI are then discussed. The advantages and drawbacks of this technology are highlighted along with future research needs.

2. SYNTHESIS OF PLANT-BASED NZVI

Plants are rich in bioactive components which act as reducing agents for the synthesis of iron nanoparticles by reducing the precursor iron compounds (Manquián-Cerda *et al.* 2017). Various plant parts such as leaf, root, stem, seed, flower, and fruit can be used to prepare the plant extract for synthesis (Poguberović *et al.* 2016). The bioactive components present in these plant parts include polyphenols, cyclic peptides, enzymes, proteins, amino acids, and other substances that do not let the particles agglomerate, thereby also acting as capping agents while working as reducing agents (Sharma *et al.* 2019). These phytochemicals present in plants are responsible for reducing Fe^{+3}/Fe^{+2} to Fe^0. Since different plants have different compositions of biomolecules present in them, the nanoparticles produced also show unique morphological characteristics making them suitable for various potential uses (Pattanayak *et al.* 2021).

Plant extracts are prepared by first cleaning the plant part with water, and then, heating it in the temperature range of 60–100 °C. The plant extract solution is then incubated and vacuum filtered, making it ready to further reduce the iron metal precursor from its multivalent form to its zerovalent state (Manquián-Cerda *et al.* 2017). The iron precursor solution is added to the plant extract and the indication of iron nanoparticles being formed is known when the solution changes its color from yellow to black (Gautam *et al.* 2018). Iron precursors such as $FeCl_3$, $FeSO_4$, and $FeCl_2$, and plant extracts with high polyphenol content are generally used for plant-based nZVI synthesis. The procedure is summarized in Figure 1.

The reduction capacity of the plant extract is mainly dependent on the number of phenolic groups (polyphenol content) present. The major class of polyphenols is flavonoids that consist of various functional groups, encouraging the formation of nanoparticles (Makarov *et al.* 2014). Based on the combination of iron precursor and plant extract pair used, reactivity is determined and nanoparticles are formed within a few minutes to a day, after plant extract is mixed in the iron precursor solution. The phenolic group of biomolecules gets complexed with iron and the biomolecules assume their oxidized ascorbic form (Kozma *et al.* 2016). The donation of electrons to free radicals from the hydroxyl group due to the conjugated π electron system of polyphenols and flavonoids enables high antioxidant activity, and so, it will prolong the life of produced nZVI (Speisky *et al.* 2022). The minimal use of chemicals, ambient room temperature and pressure, as well as easy handling

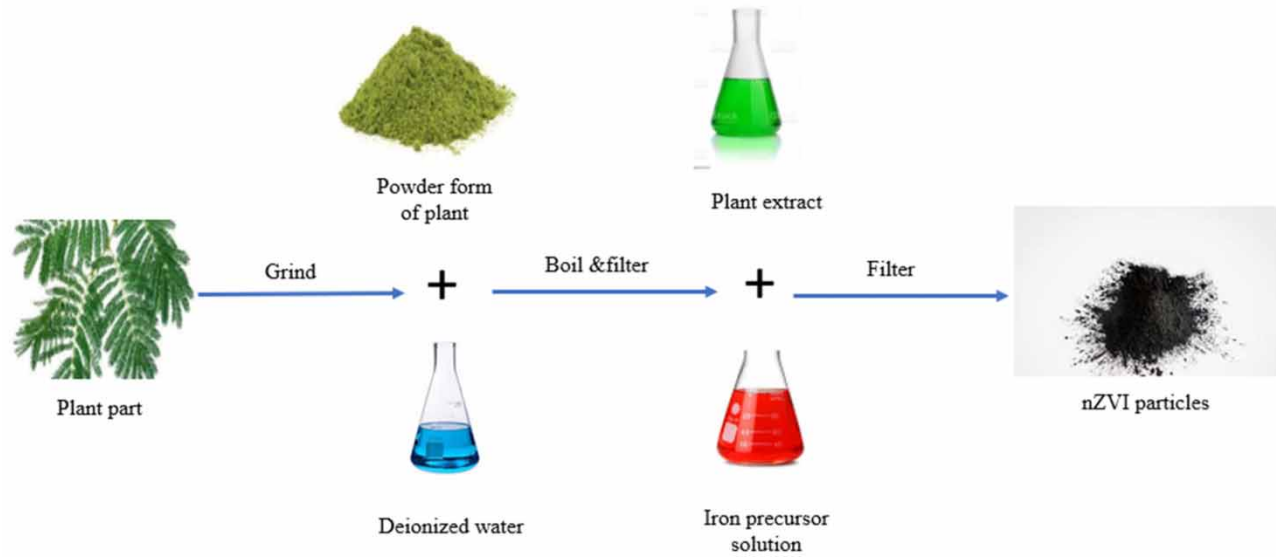

Figure 1 | Synthesis of plant-based nZVI.

and requirement of no heavy equipment for synthesis make the process economically viable for large-scale production (Nasrollahzadeh *et al.* 2021).

The mechanism of nZVI formation includes three phases namely activation phase, growth phase, and termination phase (Dikshit *et al.* 2021). In the activation phase, the metal precursor is ionized and the free positive metal ions combine with the negative biomolecule functional groups present in the plant extract. Nanoparticles are formed due to chelation and involve the reduction of multivalent iron precursor to its zerovalent form, followed by the nucleation of reduced metal atoms (Singh *et al.* 2021). The properties of nanomaterial formed depend on pH, temperature, incubation period, bioactive components in the plant and their concentration, and most importantly, the number of phenolic groups present (Shafey 2020).

The activation phase is followed by the growth phase in which the reduced and nucleated Fe ions come together to form metal nanoparticles. In this stage, the agglomeration of metal atoms takes place and the particles gain their morphological shape, while other metal atoms are still getting reduced (Khandel *et al.* 2018). Due to extended nucleation, agglomeration may lead to large particle formation, so thermodynamic energy needs to be minimized for particle stabilization to take place (Zikalala *et al.* 2018).

The last stage is the termination phase where the nanoparticles stabilize and the desired morphology of the nanoparticle is maintained owing to the formation of a layer of capping agent around the nanoparticles by improved thermodynamic stability. This capping agent is also formed from the bioactive components present in the plant and it does not allow the particles to agglomerate any further, by reducing the surface energy (Stefaniuk *et al.* 2016).

3. CHARACTERISTICS OF PLANT-BASED NZVI

Particle size, morphology, size distribution, functional groups present, composition, agglomeration, reactivity, and structure are important parameters to be evaluated before deploying nZVI in any pollution control application. These characteristics are obtained with the help of microscopic and spectroscopic techniques such as transmission electron microscopy (TEM), energy-dispersive X-ray spectroscopy (EDX), X-ray photoelectron spectrum (XPS), Fourier transform infrared spectroscopy (FTIR), dynamic light scattering (DLS), and scanning electron microscopy (SEM) (Zhou & Li 2022). A summary of the different characteristics of plant-based nZVI reported in the literature is presented in Table 1.

The images and data from TEM and SEM give information about the morphology and surface details of synthesized nZVI (Jain *et al.* 2021). The agglomeration properties of the nanoscale particles can also be interpreted from the images (Shi *et al.* 2015). It is observed that the size of plant-based nZVI is generally larger than the size of nZVI synthesized from chemical reducing agents, because the plant extract components, in addition to acting as reducing agents, also act as capping agents, forming an outer coating of biomolecule components in nZVI synthesized using plant extracts. The leaf extract of

Table 1 | Summary of the characteristics of plant-based nZVI

Plant	Plant part	Plant dose (g/L)	Synthesis temp	Time period (min)	Iron Precursor	Size (nm)	Shape	Composition	Functional groups	Structure	Surface area (m^2/g)	Pore volume (cm^3/g)	Stability	Reference
Citrus maxima	Peel	120	100 °C	80	$FeCl_3$	93.8	Irregular	Fe, N, C, O	O–H, C–H, C = O, C–N	–	–	–	Moderately stable	Wei *et al.* (2016)
Eucalyptus	Leaf	60	80 °C	60	$FeSO_4$	20–80	Spheroidal	C, O, Fe	O–H, C–H, C–H_2, C = C, C–N, C–O–C	Amorphous	–	–	–	Wang *et al.* (2014)
Juglans (Walnut)	Green skin	20	60 °C	20	$FeSO_4$	20–50	Spherical	–	O–H, C–H, C = C, Fe–O	Crystalline	–	0.38	–	Hamzezadeh *et al.* (2021)
Moringa oleifera	Peel	12	80 °C	–	$FeCl_3$	25	Irregular	Fe, C, O	O–H, C = O, C–H_2	Amorphous	–	–	Stable	Desalegn *et al.* (2019)
Calotropis gigantea	Flower	0.1	100 °C	5	$FeNO_3$	50 – 90	Spherical	Fe, O, C, P	C–O, O–H, N–H, C–H_2, C–H_3	Crystalline	–	–	Stable	Sravanthi *et al.* (2018)
Lawsonia inermis	Leaf	40	70 °C	–	$FeSO_4$	21	Distorted hexagonal	Fe, C, O, Mg, P, K	O–H, C = C, C = O,	–	–	–	–	Naseem & Farrukh (2015)
Gardenia jasminoides	Leaf	40	70 °C	–	$FeSO_4$	32	Shattered rock like	Fe, C, O, Al, Si, K	–OH, C–H, C = O, C–N, C–O	–	–	–	–	Naseem & Farrukh (2015)
Psidium guajava	Leaf	100	100 °C	20	$FeCl_3$	27	Irregular	Fe, Cl, C, O, Mn	O–H, C–O, C = O,	Crystalline	–	–	–	Jeyasundari *et al.* (2017)
Mentha piperita	Leaf	20	48 °C	5	$FeCl_3$	5 – 10	Spherical	Fe	O–H	–	–	–	–	Shad *et al.* (2020)
Urtica dioica	Leaf	50	100 °C	15	$FeCl_3$	46	Spherical	–	O–H, C–O, C = O	Amorphous	–	–	–	Ebrahiminezhad *et al.* (2017)
Ferula persica	Root	100	90 °C	60	$FeSO_4$	12.7	Spherical	C, Fe, O	–	Amorphous	46.68	0.4	stable	Huang *et al.* (2014)
Azadirachta indica	Leaf	500	50 °C	10	$FeSO_4$	–	Spherical	–	–	–	6.2	–	–	Francy *et al.* (2020)
Mentha longifolia	Leaf	500	50 °C	10	$FeSO_4$	–	Spherical	–	–	–	13	–	–	Francy *et al.* (2020)
Vitis vinifera	Leaf	20	–	–	$FeCl_3$	120 – 160	Irregular	C, O, Fe	O–H. Fe–O	Amorphous	15.08	–	–	Bhatti *et al.* (2020)
Camellia sinensis (Black tea)	Leaf	60	80 °C	60	$FeSO_4$	40 – 50	Spherical	C, O, Fe, S, Al	–	Amorphous	2.6	–	–	Huang *et al.* (2014)

Mentha piperita was used to synthesize green nZVI (Shad *et al.* 2020). The nanoparticles produced were of the size 5–10 nm with a spherical shape and showed some agglomeration. Ebrahiminezhad *et al.* (2017) used *Urtica dioica* leaves to synthesize nZVI. The TEM images showed diameters in the range of 21–71 nm with a mean diameter of 46 nm. The shape was mostly spherical, while certain oval particles were also observed. The micrographs also revealed the presence of a biological matrix around the particles because of the leaf extract. Karam *et al.* (2020) compared the characteristics of chemically synthesized nZVI and green nZVI synthesized from *Camelia sinensis* (black tea) extracts. The images of both chemically and green synthesized nZVI showed regular and irregular surfaces, and the average diameter was 40 and 80 nm, respectively. The verification of size was done using EDX, which showed a diameter of 36 nm for chemically synthesized nZVI, depicting the major content of iron in it, while the diameter of green nZVI was obtained as 83.7 nm, depicting the coating of leaf extract because of the presence of carbon and oxygen layers surrounding the particle. However, some researchers reported a smaller size for plant-based nZVI. The average diameter of chemically synthesized nZVI and nZVI synthesized from *Vaccinium corymbosum* (blueberry) extract were found to be 80.2 and 52.4 nm, respectively, by Manquián-Cerda *et al.* (2017). The conditions impacting the size and shape of synthesized nZVI include composition and concentration of extract, concentration of reagent, synthesis temperature, and reaction time (Machado *et al.* 2014).

EDX micrograph showed the chemical composition of nZVI and the surface atomic distribution (Yusmartini *et al.* 2015). Plant-based nZVI is found to have more concentrations of carbon and oxygen and a lesser concentration of iron, as compared to chemically synthesized nZVI, owing to the presence of organic substances in the biomolecules of plant extract. nZVI synthesized from green tea was characterized by EDX to determine its atomic composition (Shahwan *et al.* 2011). The spectrum peaks confirmed the presence of C (47.9%), Fe (27.8%), Na (12.5%), O (6.3%), and Cl (5.5%). The presence of Na, O, and Cl might be because of the use of NaCl and $FeCl_2$ during synthesis, while C might be because of polyphenol and some other biomolecule groups in the tea extract. Vilando *et al.* (2019) showed the use of *Euphorbia hirta linn* (Tawa-tawa) extracts for nZVI synthesis. Two types of precursors, $FeSO_4$ and $FeCl_3$, were used. The composition interpreted using EDX peaks showed the presence of Fe (43.77%) and O (56.07%) when $FeSO_4$ was the precursor, and Fe (65.97%), O (22.58%), and Cl (11.45%) were present during the synthesis with $FeCl_3$ as the precursor. The presence of Fe was attributed to the precursor used, O to phenolic compounds in plants, and Cl was found only when $FeCl_3$ was used as the precursor.

X-ray powder diffraction (XRD) is used to understand the crystalline or amorphous structure of iron nanoparticles based on the sharpness of the peaks obtained and the type of iron nanoparticles (iron oxide, iron hydroxide, zerovalent iron) based on the peaks obtained at 2θ value (Huang *et al.* 2015). Jeyasundari *et al.* (2017) used *Psidium guajava* to prepare nZVI. Using XRD, the structure was concluded to be hexagonal, based on the peaks obtained, and the size of the nanoparticles calculated, based on the width of the peak came out to be 27 nm. Machado *et al.* (2015) showed the use of various leaf extracts for nZVI synthesis. It was interpreted that nZVI produced was amorphous in nature and the heterogeneous constitution of leaves was considered to be a probable reason for it.

FTIR analysis is performed to determine the functional groups present in synthesized nZVI and those are responsible for the reduction of iron precursor. Plant-based nZVI has more carbon and oxygen functional groups owing to the biomolecules that are absent in chemically synthesized nZVI. Jha & Chakraborty (2020) studied the FTIR analysis of nZVI synthesized using *Shorea robusta* leaf extract. The functional groups found were alcohol, aldehyde, ketone, polyphenol, and alkyl groups. Alcohol and polyphenols were responsible for reducing $FeSO_4$ and acting as capping agents. The peaks obtained at 1,045 and 1,230 cm^{-1} were attributed to C–O stretching from primary alcohol, while the peak at 1,654 cm^{-1} signified the presence of C = O stretching in aldehyde and ketones. Peaks at 2,854 and 2,924 cm^{-1} showed C–H stretching of alkyl groups while peak at 3,286 cm^{-1} was owed to O–H in polyphenols. Lin *et al.* (2021) showed a comparative analysis of chemically synthesized nZVI and green nZVI synthesized from *Eucalyptus* leaves. The FTIR studies showed that chemically synthesized nZVI had very weak peaks as compared to green nZVI which had definitive peaks at 3,388 cm^{-1} showing the presence of O–H vibration, 1,636 cm^{-1} signifying C = O vibration, and 1,039 cm^{-1} stretching to the vibration of C–O–C.

Several authors used UV–visible spectral analysis to verify the reduction of Fe^{+3}/Fe^{+2} to Fe^0 with excitation at a particular wavelength of surface plasmon resonance (SPR) in nZVI (Sunardi *et al.* 2017). However, conclusive evidence on the formation of Fe(0) from Fe^{+3}/Fe^{+2} is not always obtained. nZVI synthesized from *Syzygium aromaticum* extract was shown to have its absorption peak in the range of 216–265 nm, and the synthesis was complete as shown by high band intensity with no other apparent evidence (Pattanayak *et al.* 2013). The reduction of Fe^{+2} and formation of nZVI synthesized from tea extracts was observed in the intensity of peaks at 205 and 272 nm by the excitation of surface plasmon vibrations in Fe nanoparticles, and the reduction in the intensity of peaks corresponding to tea polyphenols after the reaction with

Fe^{+2} was the only proof of formation of nZVI (Huang *et al.* 2014). In another study, Sravanthi *et al.* (2018) used *Calotropis gigantea* extract for the synthesis of nZVI, and the UV–vis absorption peaks of flower extract and nZVI synthesized from the extract were compared to understand nZVI formation. A wide range of 200–800 nm was selected for the analysis, and the peaks obtained with flower extract analysis at 300–350 nm disappeared during nZVI analysis, and broader absorption emerged at higher wavelengths which was the only evidence of nZVI formation. The characteristic UV–vis peaks were not observed for nZVI due to high iron reactivity, thereby giving no further evidence of nZVI formation (Sravanthi *et al.* 2018).

Brunauer–Emmett–Teller isotherm (BET) analysis is used to estimate the specific surface area (SSA) of synthesized nZVI. The SSA of plant-based nZVI is generally less, as compared to chemically synthesized nZVI. This might be due to the increased size of plant-based nZVI because of the biomolecule coating around it. Francy *et al.* (2020) showed the SSA of nZVI synthesized from neem and mint leaves to be 6.2 and 13 m^2/g, respectively, which was less than chemically synthesized nZVI with a SSA of 15.2 m^2/g. Raman *et al.* (2021) found the SSA of chemically synthesized nZVI and nZVI synthesized from grape leaf to be 31.04 and 15.08 m^2/g, respectively, depicting the decreased surface area of plant-based nZVI. Nasiri *et al.* (2019), however, found a higher SSA for nZVI synthesized from *Ferula persica,* as compared to chemically synthesized nZVI. The BET surface area of chemically synthesized nZVI and nZVI from plant extract were 34.38 and 46.68 m^2/g, respectively. An increased surface area generally results in better adsorption efficiency (Huang *et al.* 2014). A comparison of the properties of chemically synthesized nZVI and plant-based nZVI is presented in Table 2.

4. REMOVAL OF POLLUTANTS BY PLANT-BASED NZVI

Plant-based nZVI has been used for the removal of a variety of contaminants such as dyes, heavy metals, nutrients, and trace organics from different waste streams. This section describes these studies, highlighting the mechanisms of contaminant removal by nZVI.

4.1. Dye removal

Dyes are majorly classified as natural and synthetic dyes, based on their source material. Synthetic dyes can be divided into ionic and non-ionic categories. Ionic dyes are further classified into cationic dyes and anionic dyes which include acid, reactive, and direct dyes, while non-ionic dyes are classified into vat and dispersive dyes (Kadhom *et al.* 2020). According to their chemical structures, dyes are categorized as azo, nitro, indigoid, anthraquinone, phthalein, and triphenyl methyl dyes, based on the attached chromatograph group (Benkhaya *et al.* 2017). Reactive, direct, vat, dispersive, acid, basic, and solvent are all subgroups of dyes based on the method of application (Pandey *et al.* 2020). It is reported that discoloration and removal of

Table 2 | Comparison of the characteristics of chemically synthesized and plant-based nZVI

Characteristics	Chemical nZVI	Plant nZVI	Remarks	Reference
Size	Generally smaller	Generally larger	Polyphenol coating around nZVI nucleus increases size of plant-based nZVI Exception: Agglomeration of chemically synthesized nZVI particles increases its size	Manquián-Cerda *et al.* (2017); Raman *et al.* (2021)
Surface area and pore volume	Generally high	Generally less	Smaller average size of chemically synthesized nZVI leads to higher surface area and pore volume	Nasiri *et al.* (2019)
Composition	High Fe content	Less Fe content	Presence of organics in plant-based nZVI reduces Fe content	Shaibu *et al.* (2014)
Functional groups	Presence of less carbon–oxygen functional groups	Presence of more carbon–oxygen functional groups	Bioactive elements in plant increase C and O content	Lin *et al.* (2021)
Structure	Generally crystalline	Amorphous	Organic residues on surface causes distortion in Plant nZVI	Badmus *et al.* (2018)
Uniformity	Homogeneity	Heterogeneity	Varying amount of polyphenol in plant	Francy *et al.* (2020)

dyes can be achieved by nZVI as it is capable of destroying their chromatograph group (Pourabadeh *et al.* 2020). Plant-based nZVI shows high removal efficiency of cationic and anionic dyes consisting of attached chromatograph groups at optimum conditions. Methylene blue (MB), methyl orange (MO), and crystal violet (CV) are the most commonly studied dyes for removal by plant-based nZVI. A summary of these studies is presented in Table 3.

The adsorption capacity of plant-based nZVI is promising and is also generally higher than the conventional nZVI which is chemically synthesized. Abdelfatah *et al.* (2021b) compared the adsorption capacity of nZVI synthesized from chemical reducing agents and various plant extracts for MB removal. The adsorption capacity of chemically synthesized nZVI was 5.53 mg/g, which was much lower than those of nZVI synthesized from *Riccinus communis* and *Platanus occidentalis* with an adsorption capacity of 64.94 and 126.60 mg/g, respectively.

Various factors such as pH, contact time, adsorbent and adsorbate dose, as well as temperature, affect the adsorption capacity and removal efficiency. Hence, determining optimum conditions is important for the application of this process.

The pH at which optimum adsorption takes place depends on the properties of the dye to be adsorbed. It is known that at higher pH, the adsorbent surface is negatively charged, helping better removal of cationic dyes, and at lower pH, anionic dyes are better removed owing to the positive surface charge of the adsorbent (Bao & Zhang 2012). Shaibu *et al.* (2014) used bamboo, which is a waste agricultural product, to synthesize plant-based nZVI for the removal of MB, which is a cationic dye. The removal was less at acidic pH values. The highest removal of 79.6% was observed at a higher pH value of 11. The higher removal was attributed to the effect of alkaline pH on the charge of reactive groups in adsorbents, which is responsible for the ionization of dyes. Electrostatic attraction of opposite charges on the surface was responsible for removal.

Table 3 | Summary of parameters for dye removal using plant-based nZVI

Plant material	Dye	q_m (mg/g)	Removal (%)	Optimum conditions	Isotherm model	Kinetic model	Added reagent	References
Ricinus communis	MB	64.94	96.8	pH: 6, nZVI dose: 3 g/L, Initial dye concentration – 25 mg/L, Contact time: 1 h	Freundlich	Pseudo-first-order	–	Abdelfatah *et al.* (2021a, 2021b)
Lemon-derived waste	MB	1,959.94	96.17	pH: 11, nZVI dose: 0.5 g/L, Initial dye concentration – 1,000 mg/L, Contact time: 5 min	Freundlich and Temkin	Pseudo-second-order	$NaBH_4$	Abd El-Monaem *et al.* (2022)
Sweet-lime pulp	MB	14.76	98.9	pH: 10, nZVI dose: 1.2 g/L, Initial dye concentration – 10 mg/L, Contact time: 5 h	Freundlich and Sips	Pseudo-second-order	–	Sahu *et al.* (2019)
Ferula persica	CV	454.5	95	pH: 9, nZVI dose: 2.5 g/L, Initial dye concentration – 1,500 mg/L, Contact time: 1.5 h	Langmuir	Pseudo-second-order	β-cyclodextrin	Nasiri *et al.* (2019)
Sycamore tree seed fibers	Malachite green	43.67	96	pH: 6, nZVI dose: 1 g/L, Initial dye concentration – 100 mg/L, Contact time: 1.6 h	Langmuir	Pseudo-second-order	–	Parlayıcı & Pehlivan (2019)
Sycamore tree seed fibers	Methyl Violet	92.59	98	pH: 6, nZVI dose: 1 g/L, Initial dye concentration – 100 mg/L, Contact time: 1.6 h	Langmuir	Pseudo-second-order	–	Parlayıcı & Pehlivan (2019)
Sycamore tree seed fibers	MB	140.8	99	pH: 6, nZVI dose: 1 g/L, Initial dye concentration – 100 mg/L, Contact time: 1.6 h	Langmuir	Pseudo-second-order	–	Parlayıcı & Pehlivan (2019)
Bamboo	MB	322.6	92.3	pH: 11, nZVI dose: 0.4 g/L, Initial dye concentration – 10 mg/L, Contact time: 2 h	Langmuir and Freundlich	Pseudo-second-order	$NaBH_4$	Shaibu *et al.* (2014)

Khashij *et al.* (2020) used *Thymus vulgaris* plant-based nZVI for the degradation of an anionic dye Reactive Black 5. Dye removal was the highest at pH 4 and the reason could be attributed to electrostatic attraction. The efficiency decreased by 15% when the pH was increased to 10. At a lower pH, the formation of H^+ ions led to its reaction with nitrogen atoms of azo dye, which is favorable for Reactive Black 5 degradation by the reduction of azo bond (Quan *et al.* 2018).

The contact time for which adsorbent and adsorbate interact is an important parameter in the process design. Initially, the number of vacant sites available for adsorption on the surface of an adsorbent is more and, hence, the uptake is faster. The removal depends on the adsorbent's potential. Since with time the number of active sites saturates, the rate at which sorption takes place decreases. Thus, as time passes, adsorption still takes place until equilibrium, but the rate of removal of dye from wastewater decreases. This mechanism of higher initial uptake and subsequent decrease, until equilibrium is achieved, was shown by Parlayıcı & Pehlivan (2019) who used nZVI synthesized from *Platanus occidentalis* tree seed pod fibers for the removal of MB, malachite green oxalate (MG) and methyl violet 2B (MV) dyes. The quickest uptake took place in the first 30 min, followed by 30 min of slow uptake, and the equilibrium was reached at 70 min.

The initial concentration of dye affects its removal. Increased dye concentration results in a longer time for removal and reduction in removal efficiency. With the increment of initial dye concentration, the adsorption capacity increases until saturation due to the enhanced driving forces that surpass mass transfer resistance. Abd El-Monaem *et al.* (2022) showed a higher adsorption capacity of MB using lemon-derived biochar-based nZVI, when the initial concentration of MB was increased. The adsorption capacity increased from 495.65 to 1,864.41 mg/g when the initial MB concentration was increased from 250 to 1,000 mg/L. Sahu *et al.* (2019) used sweet-lime pulp-derived nanoparticles to remove MB. Increasing MB concentration from 10 to 40 mg/L increased the adsorption capacity from 8.2 to 32.6 mg/g.

An increase in nZVI concentration improves the dye removal efficiency with the availability of more adsorption sites and surface area, and hence, the time required decreases until saturation. After saturation, an increase in dosage does not influence the removal rate. Sahu *et al.* (2019) reported the removal of MB using sweet-lime pulp-based nZVI and showed that the removal percentage increased from 71 to 86% with the increase in adsorbent dosage from 0.4 to 1 g/L. A further increase in nZVI concentration to 1.2 g/L did not affect the removal efficiency.

Temperature is another factor that influences the adsorption process. The increase in temperature during the adsorption process increases the diffusion rate of molecules. Abd El-Monaem *et al.* (2022) used lemon-derived biochar in combination with nZVI to remove MB. The temperature was varied from 25 to 55 °C and the results clearly showed an increase in adsorption capacity and removal percentage from 957.71 mg/g and 95.58% to 997.51 mg/g and 99.74%, respectively, as the temperature increased from 25 to 55 °C. The increase in temperature leads to the increased movement of MB molecules toward the nanocomposite.

The interaction between adsorbate and adsorbent at equilibrium is determined by adsorption isotherms. The reported studies show that Langmuir and Freundlich isotherms are, generally, well-fitted for various dyes and plant-based nZVI combinations, while in certain cases, Temkin isotherms are used to model adsorption using batch tests. Abdelfatah *et al.* (2021b) reported the removal of MB dye using nZVI for *Ricinus communis* and showed that adsorption was well-fitted into Freundlich isotherm ($R^2 = 0.990$), indicating that the dye molecules adsorbed were following multilayer adsorption. The n value derived from the Freundlich isotherm equation was 1.838 indicating moderate adsorption capacity. The maximum adsorption capacity calculated from Langmuir isotherm was 61.73 mg/g. The linear plot for the Temkin adsorption isotherm suggested physical adsorption. Ahmad *et al.* (2020) showed the removal of MB dye using date palm waste. The Redlich–Peterson isotherm was the best-fitted isotherm followed by the Langmuir isotherm, indicating both heterogeneous and homogeneous adsorption. The Langmuir model predicted the maximum sorption capacity as 1,182.9 mg/g. The hydrogen bond that existed between –OH groups of sorbent and –N– groups of MB contributed to the removal. The major mechanisms for MB removal were electrostatic interactions between cationic MB and anionic surface functional group, high surface area through π-π electron donor–acceptor interactions between aromatic sorbents and cationic dye, as well as diffusion. The binding energy was very low, indicating that adsorption did not follow the ion-exchange process.

Kinetic studies have shown that the adsorption of various dyes by plant-based nZVI is, generally, well-fitted by a pseudo-second-order kinetic model. However, dye removal kinetics following pseudo-first-order and Elovich models have also been reported. Ahmad *et al.* (2020) synthesized nZVI from date palm waste and used it for the removal of MB. They found that adsorption followed pseudo-second-order ($R^2 = 0.93$–0.99) and Elovich model ($R^2 = 0.86$–0.97). The higher value of rate constants indicated chemisorption. Abdelfatah *et al.* (2021b) showed that the removal of MB, a cationic thiazine dye, using nZVI prepared from *Ricinus communis* seed extract followed the pseudo-first-order kinetic model ($R^2 > 0.97$). The values of the

kinetic constants found in the pseudo-first-order equation decreased with the increase in MB concentration indicating a physical adsorption reaction taking place. The Elovich model describes effectively the solid–liquid interaction. The value of the Elovich constants for the initial adsorption rate was higher than the desorption rate constant, indicating low desorption and a higher adsorption tendency of MB.

Several studies compared the performance of plant-based nZVI with chemically synthesized nZVI. Studies have shown plant-based nZVI as a better material for dye degradation than chemically synthesized nZVI. It is also seen that the efficiency of plant-based nZVI increases when used with some added chemicals. Nasiri *et al.* (2019) compared the efficiencies of chemically synthesized nZVI, green synthesized nZVI from *Ferula persica* extracts (G-nZVI), and green synthesized nZVI functionalized with β-cyclodextrin (β-CD) for the removal of CV dye. Chemically synthesized nZVI had a larger size as compared to the other two, which had smaller average size, higher surface area, and pore volume. It was also inferred that the removal of dye by both green synthesized nZVI particles was much more pH-dependent than chemically synthesized nZVI. The removal efficiency of 500 mg/L CV solution by chemically synthesized, green synthesized, green synthesized and functionalized with β-cyclodextrin nZVI were 7.6, 35.6, and 68.5%, respectively, at pH 9. This result validates that the use of plant root extract, instead of $NaBH_4$, results in higher dye removal because of a smaller particle size and a higher surface area. The higher removal efficiency by βCD functionalized G-nZVI compared to G-nZVI was due to the fact that βCD coating provided more adsorption sites owing to very little aggregation taking place and the presence of more than one hydroxyl group. CV inclusion via βCD hydrophobic cavity instead of just electrostatic interaction among hydroxyl groups on the surface in G-nZVI also resulted in higher dye removal.

Hydrogen peroxide acts as a Fenton reagent and increases the dye removal efficiency of plant-based nZVI when added along with it. Lim *et al.* (2018) compared nZVI synthesized using *Mulberry leaves* and nZVI synthesized using *Mulberry leaves* with added H_2O_2 for the removal of MB and MO. For a time period of 180 min and a dye dose of 5 mg/L, the removal efficiencies for MB and MO by nZVI synthesized from mulberry leaves were 39.94 and 57.32%, respectively. The removal efficiency increased to 98.77 and 98.94%, respectively, when plant-based nZVI was used along with H_2O_2, nZVI without H_2O_2 removed MO more than MB, owing to the electrostatic attraction. Hydrogen peroxide acted as a heterogeneous Fenton catalyst, producing OH radicals and accelerating the reaction rate. This shows that plant-based nZVI along with hydrogen peroxide can result in a much higher dye removal.

The mechanism involved in the removal of dyes is the reduction of dyes (breaking of chromophore group bonds) followed by adsorption. During the reaction of nZVI with dye molecules, ZVI gets oxidized to Fe^{+2} or Fe^{+3} ions, thereby emitting electrons. The ferric ions form hydroxide when reacting with water and release H^+ and H radicals. These emitted electrons are accepted by dye molecules and they get reduced into intermediate products (Simseka *et al.* 2017). This reduction process breaks the chromophore group bonds in the dye. The reaction of these generated hydrogen ions and free radicals with oxygen present forms hydrogen peroxide (Donadelli *et al.* 2018). Hydrogen peroxide with ferrous ions creates Fenton-like reactions, releasing hydroxyl free radicals that decolorize dyes by reacting with chromophores (Wu *et al.* 2014). It could also be inferred that nZVI in Fenton conditions would help in better degradation of dyes, as more and faster reduction of dyes could take place in the presence of hydroxyl free radicals. Followed by this reduction process, adsorption takes place. Ferric hydroxide compounds form a passive iron oxide layer and the intermediate dye compounds can be adsorbed (Liu *et al.* 2017). Electrostatic interaction and π-π electron donor–acceptor reactions are also involved in the adsorption process (Mu *et al.* 2017). The schematic diagram of the mechanisms involved in the dye removal by nZVI is presented in Figure 2.

4.2. Heavy metal removal

Industries such as pesticides, paints, mining, electroplating, ceramics, electronic products, and metal alloys use heavy metals in huge quantities and the effluent generated from these industries is considered as the main source of heavy metal generation (Li *et al.* 2017b). Because of industrial discharges, elevated levels of heavy metals are found in most groundwater and surface water (Angaru *et al.* 2021). Metals such as iron, zinc, chromium, lead, and copper are essential to a certain limit in the human body for biochemical and physiological functioning, but in excess quantities, they produce various adverse health impacts (Latif *et al.* 2020). These heavy metals impact the environment because of their toxicity and non-biodegradability. For example, Pb(II) affects the kidneys and reproductive system in humans (Ali *et al.* 2019). Cr(VI) is highly soluble, carcinogenic, and teratogenic (Samuel *et al.* 2021). Considering the threat of such heavy metals in the ecosystem, their removal is inevitable. Plant-based nZVI has shown the capability of removing various heavy metals such as lead, mercury, arsenic, chromium,

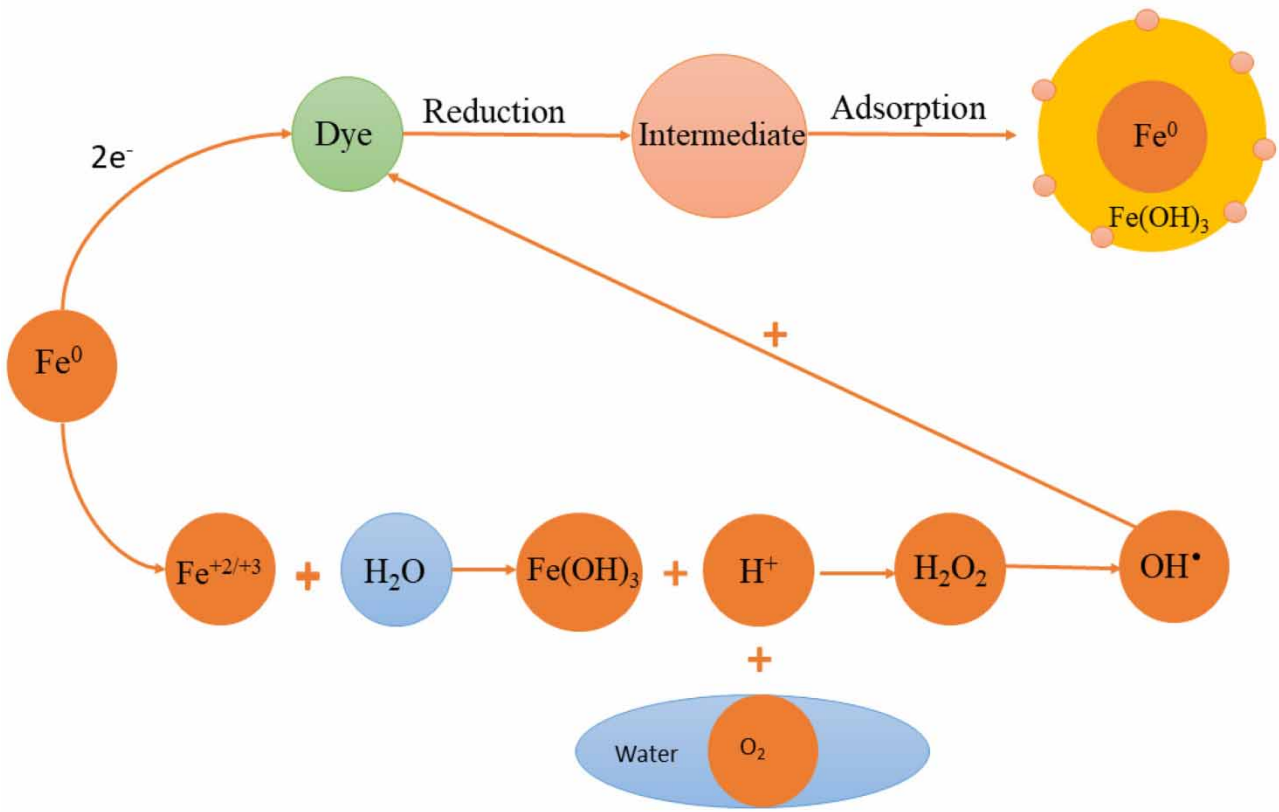

Figure 2 | Schematic on the mechanisms of dye removal using plant-based nZVI.

copper, nickel, and cadmium. This section discusses these studies and a summary of the reported studies is presented in Table 4.

High adsorption capacity has been observed for plant-based nZVI for different heavy metals. Mulberry-based nZVI was found to have an As(III) adsorption capacity of 1,329 mg/g and cherry leaves-based nZVI had an adsorption capacity of 904.1 mg/g for Cr(VI) (Poguberović *et al.* 2016). The adsorption capacity of plant-based nZVI for metals has been observed to be higher than that of chemically synthesized nZVI. Du *et al.* (2023) showed that nZVI synthesized from green tea extracts had an adsorption capacity seven times higher for Pb(II) compared to chemically synthesized nZVI. They also found better removal efficiency when $Fe_2(SO_4)_3$ was used as the precursor iron in plant-based nZVI, compared to $FeSO_4$. The adsorption capacity was 377.3 mg/g when $Fe_2(SO_4)_3$ was used, which was higher than 327.6 mg/g for nZVI synthesized using plant extract and $FeSO_4$, owing to easier agglomeration of $FeSO_4$ particles. Arshadi *et al.* (2017) reported that *Azolla filiculoides*-based nZVI had an adsorption capacity of 459.3 mg/g for Hg(II) and 462.7 mg/g for Pb(II).

Studies have been conducted on the effect of various factors such as pH, contact time, temperature, adsorbent and adsorbate dosages that affect the adsorption process of heavy metals by plant-based nZVI. The optimum pH is dependent on parameters like functional groups present in nZVI, which in turn, is dependent on the type of plant selected, charge on the pollutant to be removed, and electrostatic interaction.

Rana *et al.* (2018) studied the oxidation of As(III) using nZVI synthesized from guava leaves at different pH values. At pH 3, in the first 2 min itself, 70% of As(III) was oxidized to As(V) owing to a Fenton-like reaction at acidic pH and prevention of the formation of coating of an oxide layer, which could otherwise hinder adsorption. At neutral pH, 30% oxidation took place in 2 min and 74% in 10 min. After the first 2 min, no significant oxidation was observed owing to the competition of As(III) and As(V) for the available active binding sites. At pH 9, the removal through oxidation decreased drastically to 25% as ferrous and ferric hydroxides were formed on the surface, thereby decreasing the active sites for adsorption. They also suggested that at high pH, polyphenols in the plant extract get ionized, thereby causing the capping agents to be unavailable. Due to this, ZVI reacts with atmospheric oxygen forming hydroxides. Hence, a lower pH gives better efficiency.

Table 4 | Summary of the studies on the removal of heavy metal using plant-based nZVI

Plant material	Heavy metal	q_m (mg/g)	Removal (%)	Optimum conditions	Kinetics model	Isotherm model	Added reagent	Reference
Guava	As(III)	–	74	pH: 7, nZVI dose: 2 g/L, Initial heavy metal concentration: 1 mg/L, Contact time: 10 min	First-order	–	–	Rana *et al.* (2018)
Blueberry	As(V)	57.1	70	pH: 3, nZVI dose: 2.5 g/L, Initial heavy metal concentration: 200 mg/L, Contact time: 120 min	Pseudo-second-order	Langmuir-Freundlich	–	Manquián-Cerda *et al.* (2017)
Europhyla-Eucalyptus	As(V)	21.59	55.9	pH: 6, nZVI dose: 1 g/L, Initial heavy metal concentration: 1 mg/L, Contact time: 24 h	Pseudo-second-order	Langmuir	–	Wu *et al.* (2019)
Azolla filiculoides	Pb(II)	462.7	97.20	pH: 7, nZVI dose: 1 g/L, Initial heavy metal concentration: 100 mg/L, Contact time: 20 min	Pseudo-second-order	Langmuir	NaOH + $NaBH_4$	Arshadi *et al.* (2017)
Azolla filiculoides	Hg(II)	459.3	95.70	pH: 7, nZVI dose: 1 g/L, Initial heavy metal concentration: 100 mg/L, Contact time: 20 min	Pseudo-second-order	Langmuir	NaOH + $NaBH_4$	Arshadi *et al.* (2017)
Green tea	Pb(II)	100	97.50	pH: 5, nZVI dose: 0.5 g/L, Initial heavy metal concentration: 50 mg/L, Contact time: 20 min	Pseudo-second-order	Langmuir	–	Lin *et al.* (2020)
Rosa damascene	Cr(VI)	453.7	94.87	pH: 2, nZVI dose: 0.2 g/L, Initial heavy metal concentration: 100 mg/L, Contact time: 1 min	Pseudo-second-order	–	–	Fazlzadeh *et al.* (2017)
Thymus vulgaris	Cr(VI)	466	86.8	pH: 2, nZVI dose: 0.2 g/L, Initial heavy metal concentration: 100 mg/L, Contact time: 1 min	Pseudo-second-order	–	–	Fazlzadeh *et al.* (2017)
Urtica dioica	Cr(VI)	462	83.48	pH: 2, nZVI dose: 0.2 g/L, Initial heavy metal concentration: 100 mg/L, Contact time: 1 min	Pseudo-second-order	–	–	Fazlzadeh *et al.* (2017)
Eucalyptus	Cr(VI)	149.3	75.1	pH: 3, nZVI dose: 0.5 g/L, Initial heavy metal concentration: 15 mg/L, Contact time: 60 min	Pseudo-first-order	Freundlich	–	Weng *et al.* (2016)
Eucalyptus	Cu(II)	163.9	64.2	pH: 7, nZVI dose: 0.5 g/L, Initial heavy metal concentration: 15 mg/L, Contact time: 60 min	Pseudo-first-order	Freundlich	–	Weng *et al.* (2016)
Barberry	Cr(VI)	–	–	pH: 2, nZVI dose: 0.5 g/L	Pseudo-second-order	–	–	Samadi *et al.* (2021)
Mulberry	As(III)	1,329	–	pH: 8, Initial heavy metal concentration: 10 mg/L	Pseudo-second-order	Freundlich	–	Poguberović *et al.* (2016)
Cherry	Cr(VI)	904.1	–	pH: 7, Initial heavy metal concentration: 10 mg/L	Pseudo-second-order	Freundlich	–	Poguberović *et al.* (2016)

(*Continued.*)

Table 4 | Continued

Plant material	Heavy metal	q_m (mg/g)	Removal (%)	Optimum conditions	Kinetics model	Isotherm model	Added reagent	Reference
Camellia sinensis	As(V)	18.98	–	nZVI dose: 1 g/L, Initial heavy metal concentration: 10 mg/L	Pseudo-second-order	Langmuir	–	Kamath *et al.* (2020)
Quercus virginiana	As(V)	32.05	–	nZVI dose: 1 g/L, Initial heavy metal concentration: 10 mg/L	Pseudo-second-order	Langmuir	–	Kamath *et al.* (2020)
Punica granatum	As(V)	11.65	–	nZVI dose: 1 g/L, Initial heavy metal concentration: 10 mg/L	Pseudo-second-order	Langmuir	–	Kamath *et al.* (2020)

Higher removal of heavy metals at higher pH has also been reported. Arshadi *et al.* (2017) found a higher removal of heavy metals such as Pb(II) and Hg(II) in the pH range of 5–9. At a higher pH, the surface of the adsorbent became negatively charged causing precipitation of $Pb(OH)_2$ and protonation/deprotonation of hydroxyl species on the nZVI surface. Although uptake was high at alkaline pH, the formation of iron hydroxides hindered the uptake.

The removal of pollutants increases with the increase in contact time, until an equilibrium is achieved. After that point, the uptake is negligible due to the filling of all vacant active sites on the adsorbent. As the adsorbent dose increases, the uptake increases, owing to the availability of more active sites for adsorption. However, increasing it above a certain limit could cause agglomeration of nZVI particles, thereby decreasing efficiency. At an increased pollutant concentration, more time for removal is required, and this would also cause less removal, as the pollutant would occupy the vacant sites on the adsorbent faster (Yan *et al.* 2012).

The adsorption isotherm that better fits the adsorption by plant-based nZVI was mostly Langmuir or Freundlich. Poguberović *et al.* (2016) showed the use of oak, mulberry, and cherry leaves nZVI for the removal of As(III) and Cr(VI). For isotherm studies, the coefficients indicated that the data better fitted Freundlich isotherm for the removal of both As(III) and Cr(VI), indicating multilayer adsorption. Weng *et al.* (2016) used Eucalyptus leaf-based nZVI for the removal of Cr(VI) and Cu(II). The adsorption isotherm coefficients calculated from experimental data showed that the data better fits the Freundlich model. Since the value of coefficient n exceeded 1, the adsorption was regarded as chemisorption, showing a high affinity between the adsorbate and the adsorbent. The highest adsorption capacity obtained at 308 K for Cr(VI) and Cu(II) were found to be 149.3 and 163.9 mg/g, respectively. They also showed that *Eucalyptus*-based nZVI had the potential to remove Zn(II) and Pb(II), along with Cr(VI) and Cu(II) from electroplating wastewater. The use of *Eucalyptus*-based iron nanoparticles for the removal of various heavy metals has been reported by various studies. Kamath *et al.* (2020) used *Eucalyptus* leaves and other plants' leaves such as black tea, oak, green tea, and pomegranate leaves for the removal of arsenic from water. *Eucalyptus* leaves showed the fastest adsorption with an adsorption capacity of 39.84 mg/g. The Langmuir isotherm fitted into the data well, indicating monolayer adsorption.

It has been known from various studies that the adsorption of heavy metals by plant-based nZVI generally follows pseudo-second-order kinetics, indicating the rate-limiting step to be chemisorption. However, certain exceptions are also observed. Poguberović *et al.* (2016) showed the removal of As(III) and Cr(VI) using oak, mulberry, and cherry leaf-based nZVI. The pseudo-second-order kinetic model was proved to be a better fit and the mechanisms involved were adsorption, reduction, metal-nZVI interactions like oxidation/re-oxidation and co-precipitation of As(III). The use of *Eucalyptus* leaf for the synthesis of iron nanoparticles for the removal of mixed contaminants was shown by Weng *et al.* (2016). Since the removal mechanism was not only attributed to adsorption but also reduction, the kinetics for both adsorption and reduction were studied separately. The study showed Cr(VI) and Cu(II) removal efficiency of 74.2 and 45.2% in separate solutions which decreased to 58.9 and 33%, respectively, owing to the competition in occupying active sites during adsorption and reduction. The adsorption kinetics study showed that the adsorption fitted well to the pseudo-second-order, while the reduction kinetics study showed that the removal due to functional iron nanoparticles was well-fitted to the pseudo-first-order model. Hence, sorption kinetics followed pseudo-second-order, while reduction followed pseudo-first-order, in this case.

The mechanisms involved in the removal of heavy metals with nZVI include adsorption, absorption, precipitation, co-precipitation, oxidation, and reduction. The predominant mechanism depends on the redox nature of the pollutant and solution pH, as well as ionic strength and dosage of the adsorbent (Yan *et al.* 2012). The removal of arsenate using blueberry leaves-supported nZVI also showed the formation of transitional compounds during removal, along with different removal mechanisms as mentioned above, due to the various oxidation states of iron (Manquián-Cerda *et al.* 2017).

4.3. Nutrient removal

Wastewater discharges containing inorganic nutrients like nitrogen and phosphorus disposed in aquatic bodies cause eutrophication, which is one of the most prevalent global water pollution problems (Jiang *et al.* 2019). Increased use of mineral and organic fertilizers and generation of higher quantities of industrial and municipal sludge are factors responsible for nitrogen and phosphorus in the wastewater discharged (Kończak & Huber 2022). Eutrophication promotes algal bloom which results in increased oxygen consumption, which in turn, causes aquatic and ecosystem imbalance (Govarthanan *et al.* 2020). It also causes loss of biodiversity, reduced visual amenity, unpleasant odor, toxin production, and impaired habitat for fish species (Abell *et al.* 2022). Water with an excess amount of nutrients, if consumed, poses threats to human health, along with ecosystem imbalance; hence, nutrient removal is necessary. Plant-based nZVI is capable of removing nutrients like nitrogen and phosphorous in their various forms. Table 5 presents the summary of some of the recent studies on nutrient removal by plant-based nZVI.

The adsorption capacity of chemically synthesized nZVI for nutrients is generally higher than plant-based nZVI. Wang *et al.* (2014) showed the equilibrium adsorption capacity of chemical nZVI to be 20.95 mg/g and that of green tea and *Eucalyptus*-based nZVI to be 13.06 and 9.69 mg/g, respectively, for nitrate. On the other hand, plant-based nanoparticles are seen to be less effective for the removal of nutrients as compared to chemically synthesized nanoparticles. Prabhakar *et al.* (2017) showed the removal of nitrate and phosphate by chemically synthesized nZVI to be 85.27 and 67.98%, respectively, while *Eichhornia crassipes*-based nZVI was able to remove 74.52% nitrate and 55.39% phosphate.

The adsorption capacity changes with variation in pH are based on the chemistry between the functional groups and the reaction behavior of the adsorbent and the adsorbate. Devatha *et al.* (2016) showed the removal of total phosphate and nitrate using leaf extracts of *Mangifera indica*, *Murraya koenigii*, *Azadiracta indica,* and *Magnolia champaca*. For phosphate, which is in anionic form, the removal was better at a lower pH, as in that condition iron nanoparticles are in the cationic form, making the removal effective by electrostatic attraction. Hence, in the pH range of 3.5–5.5, the removal efficiency of phosphate was 90% by *Mangifera indica, Murraya koenigii,* and *Magnolia champaca*-based nZVI. However, for the *Azadiracta indica* plant-based nZVI, at a pH of 7.5, high phosphate removal efficiency (98%) was observed, which may be due to the presence of various polyphenols, making the adsorption more efficient. Nitrate removal was observed to be better by all the aforementioned plant-based nZVI at a pH of 6.5–8.0, owing to the presence of more polyphenols, and the removal mechanism was concluded to be adsorption and co-precipitation.

Most reported studies show better removal as temperature increases, but there are exceptions depending on the nutrient to be removed and the bond between the adsorbent and the adsorbate. If the removal is improved with increasing temperature, the reaction is endothermic. Cao *et al.* (2016) showed the removal of phosphate using nanoparticles synthesized by *Eucalyptus* leaf extract, along with the use of CTAB (cetyltrimethylammonium bromide) as a stabilizer in the green synthesis process. Based on batch experiments with 20 mg/L of phosphate at different temperatures of 288, 298, and 308 K, the phosphate uptake values were 5.64, 7.94, and 9.41 mg/g, respectively, which indicated that an increase in the temperature led to an increased adsorption capacity, within a few minutes itself. The increased adsorption uptake is supported with a thermodynamic study. The results showed a positive value of enthalpy ($\Delta H = 119.15$ kJ/mol) indicating an endothermic process. The value of ΔG (Gibbs free energy) decreased from -2.81 to -11.3 kJ/mol with the increase in temperature (288–308 K), showing spontaneity in the adsorption process. The positive value of entropy ($\Delta S = 422.55$ J/k mol) showed increased randomness at the solid–liquid interface during adsorption. These phenomena are because of the increase in activation energy, causing an increased reaction velocity, making the uptake easier with temperature increase. The mechanism associated with adsorption here was an inner-sphere complexing mechanism and electrostatic attraction.

Xu *et al.* (2020) showed ammonia and phosphate removal using nanoparticles synthesized from *Eucalyptus* leaves with zeolite as a supporter. Batch experiments for 10 mg/L concentration for simultaneous removal of NH_4^+ and PO_4^{-3} were performed at various temperatures of 20, 30, and 40 °C. Ammonia removal decreased with an increase in temperature, suggesting the process to be exothermic. The increase in temperature did not directly contribute to the adsorption of phosphate, but

Table 5 | Summary of the studies on the removal of nutrients using plant-based nZVI

Plant material	Nutrient	q_m (mg/g)	Removal (%)	Optimum conditions	Kinetics model	Isotherm model	Added reagent	Reference
Green tea	NO_3^-	13.06	60%	pH: 8.45, nZVI dose: 1 g/L, Initial nutrient concentration: 20 mg/L, Contact time: 90 min	Pseudo-second-order	-		Wang *et al.* (2014)
Eucalyptus	NO_3^-	9.698	41.40%	pH: 8.45, nZVI dose: 1 g/L, Initial nutrient concentration: 20 mg/L, Contact time: 90 min	Pseudo-second-order	–		Wang *et al.* (2014)
Eucalyptus	PO_4^{-3}	18.69	97.30%	pH: 1–9, nZVI dose: 2 g/L, Initial nutrient concentration: 20 mg/L, Contact time: 90 min	Pseudo-second-order	Langmuir	CTAB	Cao *et al.* (2016)
Eucalyptus	NH_4^+	3.47	43.30%	pH: 4, nZVI dose: 7 g/L, Initial nutrient concentration: 10 mg/L, Contact time: 30 min	Pseudo-second-order	Langmuir	Zeolite	Xu *et al.* (2020)
Eucalyptus	PO_4^{-3}	38.91	99.80%	pH: 8, nZVI dose: 7 g/L, Initial nutrient concentration: 10 mg/L, Contact time: 30 min	Pseudo-second-order	Langmuir	Zeolite	Xu *et al.* (2020)
Azadiracta indica	PO_4^{-3}	–	98.08%	pH: 7.5, Initial nutrient concentration: 92.5 mg/L, Contact time: 13 days	–	–	–	Devatha *et al.* (2016)
Azadiracta indica	NH_4^+	–	84.32%	pH: 6.5–8, Initial nutrient concentration: 44.46 mg/L, Contact time: 13 days	–	–	–	Devatha *et al.* (2016)
Eichhornia crassipes	NO_3^-	–	74.52%	Initial nutrient concentration: 14.77 mg/L, Contact time: 5 days	–	–	–	Prabhakar *et al.* (2017)
Mimosa Pudica	NO_3^-	–	65.23%	Initial nutrient concentration: 14.77 mg/L, Contact time: 5 days	–	–	–	Prabhakar *et al.* (2017)
Lantana camara	PO_4^{-3}	–	53.68%	Initial nutrient concentration: 23.5 mg/L, Contact time: 5 days	–	–	–	Prabhakar *et al.* (2017)
Eucaluptus	N	–	71.70%	Initial nutrient concentration: 25.57 mg/L, Contact time: 21 days	–	–	–	Wang *et al.* (2014)
Eucaluptus	P	–	30%	Initial nutrient concentration: 10.55 mg/L, Contact time: 5 days	–	–	–	Wang *et al.* (2014)
Banana	NO_3^-	–	88.00%	nZVI dose: 9.5 mg/L, Initial nutrient concentration: 20 mg/L, Contact time: 5 min	Pseudo-second-order	Langmuir	–	Abida *et al.* (2022)
Mango	PO_4^{-3}	–	78.00%	nZVI dose: 9.5 mg/L, Initial nutrient concentration: 20 mg/L, Contact time: 4 h	Pseudo-second-order	Langmuir	–	Abida *et al.* (2022)
Pomegranate	PO_4^{-3}	–	88.00%	nZVI dose: 9.5 mg/L, Initial nutrient concentration: 20 mg/L, Contact time: 4 h	Pseudo-second-order	Langmuir	–	Abida *et al.* (2022)

reduced the equilibrium time. For both NH_4^+ and PO_4^{-3}, ΔH was negative with values of −3.40 and −10.51 kJ/mol, respectively, indicating the reaction to be exothermic. The positive values of ΔS, 0.0096 for NH_4^+, and 0.0049 for PO_4^{-3} showed that the solid–liquid interface degree of disorder decreased during the reaction. ΔG values were negative at all temperatures, showing the adsorption to be spontaneous and favorable. The results of experimental data showed that the mechanism of adsorption of NH_4^+ was physical adsorption via electrostatic attraction, while that of PO_4^{-3} was chemisorption, wherein removal takes place by an exchange between Fe–OH formed and phosphate.

Studies show that the ability of nanoparticles synthesized from plant extract for nutrient uptake decreases as they age. The freshly synthesized plant-based nano-zerovalent iron shows a better removal efficiency as compared to aged nanoparticles.

Prabhakar *et al.* (2017) showed the use of aquatic and terrestrial weed-based plants for nZVI synthesis. The synthesized nanoparticles showed high efficiency for nitrate and phosphate removal. *Eichhornia crassipes, Lantana camara, Mimosa pudica,* and chemically synthesized nZVI showed a nitrate removal efficiency of 74.52, 71.12, 65.23, and 85.27% and a phosphate removal efficiency of 55.39, 53.68, 46.23, and 67.98%, respectively. Green synthesized nZVI was left open for 15 days, and then, its efficiency was slightly lower with nitrate removal of 67.21, 66.29, 57.53 and 63.21% and phosphate removal of 43.67, 40.53, 38.17 and 39.32%, respectively.

The kinetics followed by plant-based nZVI for the removal of nutrients is seen to fit well in the pseudo-second-order model. Wang *et al.* (2014) used green tea and *Eucalyptus* leaves to synthesize nZVI for the removal of nitrates. The use of these plant-based nZVI was successful as green tea-based nanoparticles removed 59.7% and *Eucalyptus* leaves-based nanoparticles removed 41.4% of nitrates present in wastewater. They also compared the removal with chemically synthesized nZVI, whose removal efficiency was 87.6%, which was more than green nZVI. The adsorption capacity at equilibrium was 13.06 and 9.698 mg/g for green tea and *Eucalyptus* nanoparticles, respectively. The major mechanisms responsible here were reduction by nZVI along with adsorption and co-precipitation.

Batch adsorption experiments showed the Langmuir adsorption isotherm in the majority of analyses. Abida *et al.* (2022) studied the removal of nitrates and phosphates using green synthesized nZVI from peels of mango, banana, and pomegranate. The Langmuir isotherm was proved to be best fitted for the adsorption of phosphates at various concentrations, with an equilibrium time of 60 min. The maximum adsorption capacity was found to be higher for nZVI prepared from pomegranate peels (68.45 mg/g), followed by banana and mango peels, with values of 35.71 and 24.39 mg/g, respectively. The adsorption kinetics followed pseudo-second-order and the small value of rate coefficient k showed the process to be slow.

The removal of nutrients from wastewater using plant-based nZVI involves electrostatic attraction, adsorption, and co-precipitation (Cao *et al.* 2016). Xu *et al.* (2020) showed interactions between NH_4^+ and PO_4^{-3}, and *Eucalyptus*-based nZVI supported by Zeolite, with electron sharing or ligand exchange mechanisms. Prabhakar *et al.* (2017) showed that the removal of nitrate and phosphate from chemically synthesized nZVI involved a reduction mechanism, making it better than *Eichhornia crassipes, Lantana camara,* and *Mimosa pudica*-based nZVI, which involved adsorption and co-precipitation mechanisms because of the presence of polyphenols as the capping layer.

4.4. Trace organic compounds removal

Trace organic compounds are organic compounds that are natural or synthetic, mostly non-biodegradable, and cause harm as they are hazardous even at low concentrations (Tufail *et al.* 2020). They include pesticides, endocrine-disrupting chemicals, personal care products, pharmaceutical chemicals, disinfection, and industrial wastewater by-products (Shin *et al.* 2022). The presence of these trace organics is known to disrupt the aquatic ecosystem along with having a highly negative impact on humans and wildlife (Alexander *et al.* 2012). Trace organics have various functional groups like electron donating or electron accepting that have the property of being toxic, recalcitrant, and resistant to the basic physicochemical and biological processes, hence, requiring advanced processes for their removal (Li *et al.* 2022). Plant-based nZVI has been studied for removing major pharmaceutical compounds among the different classes of trace organics, and these studies are summarized in Table 6.

As observed from the literature, low pH gives better removal of pharmaceutical compounds. Demirezen *et al.* (2019) showed the removal of amoxicillin using green nanoparticles synthesized from *Ceratonia siliqua* (Carob pod). The removal was tested at various pH values. The results showed the highest removal efficiency of 99% at pH 2. At higher pH, inactivation of active sites takes place and a passive oxide layer is formed on the surface, decreasing the adsorption capacity. It was also observed that for a time period of 80 min, the removal was more at pH 5, owing to electrostatic interactions, but at a longer contact time, pH 2 also gave high removal efficiency. Jha & Chakraborty (2023) showed the removal of tetracycline and ciprofloxacin antibiotics using *Shorea robusta* leaf extract. Removal efficiencies of 82.3 and 77.9% were observed at pH 6 for tetracycline and ciprofloxacin, respectively. A high removal efficiency was observed in the pH range of 4–8.

Batch studies are performed to understand the removal process. Since the trace organics group includes major chemicals with varying functional groups, the adsorption isotherm also varies with each individual case, depending on the chemicals, functional groups, and electrostatic nature of the adsorbent and the adsorbate. Leili *et al.* (2018) prepared nZVI using nettle and thyme leaf extracts for the removal of antibiotic cephalexin. The experimental data fitted well in the Freundlich model ($R^2 = 0.992$) for nettle leaf with a maximum adsorption capacity of 1,667 mg/g, indicating a heterogeneous adsorbent surface and multilayer adsorption. The adsorption isotherm for removal by thyme-based nZVI fitted better to the Langmuir model

Table 6 | Summary of the studies on the removal of trace organic compounds using plant-based nZVI

Plant material	Trace organic compound	q_m (mg/g)	Removal (%)	Optimum pH	Kinetics model	Isotherm model	Added reagent	Reference
Tea	Rifampicin	107.7	69	pH: 5, nZVI dose: 0.5 g/L, Initial trace organic compound concentration: 50 mg/L, Contact time: 20 min	–	–	–	Lin *et al.* (2020)
Phoenix dactylifera	Ciprofloxacin	92	–	pH: 7, nZVI dose: 0.15 g/L, Initial trace organic compound concentration: 30 mg/L, Contact time: 15 min	Pseudo-second-order	Hill	–	Shanableh *et al.* (2021)
Nettle	Cephalexin	1,667	90	pH: 2, nZVI dose: 0.1 g/L, Initial trace organic compound concentration: 25 mg/L, Contact time: 20 min	Pseudo-first-order	Freundlich	–	Leili *et al.* (2018)
Thyme	Cephalexin	1,428	84	pH: 2, nZVI dose: 0.1 g/L, Initial trace organic compound concentration: 25 mg/L, Contact time: 20 min	Pseudo-first-order	Langmuir	–	Leili *et al.* (2018)
Black tea	Sulphadiazine	–	90	Initial trace organic compound concentration: 50 μmol/L, Contact time: 1 h	–	–	H_2O_2	Conde-Cid *et al.* (2021)
Black tea	Sulphadiazine	–	69	Initial trace organic compound concentration: 50 μmol/L, Contact time: 8 days	–	–	–	Conde-Cid *et al.* (2021)
Ricinus communis	Tetracycline	72.64	98	pH: 6, nZVI dose: 3 g/L, Initial trace organic compound concentration: 25 mg/L, Contact time: 45 min	Pseudo-second-order	Langmuir	–	Abdelfatah *et al.* (2021b)
Ceratonia siliqua	Amoxicillin	–	99	pH: 2, nZVI dose: 0.04 g/L, Initial trace organic compound concentration: 5 mg/L, Contact time: 200 min	Pseudo-first-order	–	–	Demirezen *et al.* (2019)
Shorea robusta	Tetracycline		88	pH: 4–6, nZVI dose: 0.014 g/L, Initial trace organic compound concentration: 15 mg/L, Contact time: 70 min	Pseudo-second-order	–	–	Jha & Chakraborty (2023)
Shorea robusta	Ciprofloxacin		84	pH: 4–6, nZVI dose: 0.0175 g/L, Initial trace organic compound concentration: 25 mg/L, Contact time: 70 min	Pseudo-second-order	–	–	Jha & Chakraborty (2023)

($R^2 = 0.994$), indicating monolayer adsorption with a maximum adsorption capacity of 1,428 mg/g. Abdelfatah *et al.* (2021b) used nZVI synthesized from *Riccinus communis* for the removal of tetracycline. The value of R^2 was highest for the Langmuir model, suggesting it to be the best fit. The maximum adsorption capacity of 72.64 mg/g was achieved with 98% removal in 45 min. Adsorption and reduction were the mechanisms of removal.

Leili *et al.* (2018) used nettle and thyme-based nZVI for the removal of cephalexin. The pseudo-first-order kinetics model was a better fit, based on the experimental data for both the adsorbents. The coefficients suggested that diffusion through the boundary liquid layer around the adsorbent was the main controlling step because the R^2 value of film diffusion was higher than that of intra-particle diffusion. Adsorption was favorable as values of constant n in the Freundlich equation were 0.501 and 0.505 for nettle and thyme nZVI, respectively. Abdelfatah *et al.* (2021b) used *Riccinus communis*-based nZVI for the removal of tetracycline. The experimental data of removal well-fitted to the pseudo-second-order kinetic model. The decreasing value of the kinetic coefficient showed that the removal was a physical adsorption process. Generally, van der Waal's forces are responsible for physical adsorption requiring very less adsorption energy.

The two major mechanisms for the removal of trace organics are adsorption or adsorption followed by reduction. Conde-Cid *et al.* (2021) showed the use of black tea leaves and vineyard pruning residue to synthesize nZVI for the removal of sulfadiazine, which is a sulfonamide antibiotic. They aimed at quantifying the removal, owing to adsorption alone and a combination of adsorption and reduction. These two experiments were distinguished by preparing two types of green nZVI. The first nZVI was made unreactive by exposing it to atmospheric oxygen so that all the uptake would be due to adsorption and the second type was reactive nZVI capable of reacting with the adsorbate, and hence, the removal of antibiotic would be done because of adsorption and reduction. Hydrolysis and biodegradation were not the removal mechanisms here, as there was no removal of sulfadiazine without the presence of green nZVI. For unreactive nZVI, the highest removal efficiency for maximum dose was 58% showing removal via adsorption mechanism, while it was 69% when reactive nZVI was used showing reductive degradation as the dominant mechanism in the initial phase, followed by adsorption. A long contact time of 192 h was required. They also showed the increase in removal efficiency to be 90% and the drastic decrease in contact time to be 1 h, when H_2O_2 was used as the catalyst for the Fenton reaction, and further showed that the use of green nZVI in simulated sunlight would highly enhance the removal process by giving a complete removal in 5 min.

5. REUSABILITY

Regeneration and reusability of synthesized nZVI are important to have a sustainable life and to make it environment friendly and cost-effective (Li *et al.* 2023). The regeneration method generally used is chemical regeneration, wherein the removal of contaminants from exhausted nZVI is done by the ion-exchange process when washed with a chemical solvent (Rashtbari *et al.* 2020). The different solvents commonly used to remove the contaminants from the surface of plant-based nZVI include NaOH, HCl, EDTA, H_2SO_4, HNO_3, $NaNO_3$, and Ca $(NO_3)_2$ (Hassan *et al.* 2020). Once treated with the solvent, the adsorbent is ready to be reused, although the efficiency decreases after a few cycles because of the reduction in active sites of the adsorbent and the change in their physicochemical properties (Pourali *et al.* 2022).

Lin *et al.* (2020) studied the removal of heavy metal Pb(II) and trace organic rifampicin using nZVI synthesized from tea extracts. Regeneration using three different solutions, 0.1 M HCl, absolute ethanol, and deionized water was attempted. The removal efficiency was high even after five cycles. The removal of Pb(II) and rifampicin was 52.3 and 64.9%, respectively, after five cycles, as compared to 97.5 and 68.8% in the first cycle. The use of kaolin-supported green nZVI prepared from *Ruellia tuberosa* leaves for decolorization of azo dye was shown by Khunjan & Kasikamphaiboon (2021). The removal efficiency in the first cycle was 99.7% which decreased to 88.6% in the fifth cycle when used after regeneration. Fatimah *et al.* (2020) showed the synthesis of nanoparticles using *Parkia speciosa Hassk* pod for the degradation of bromophenol blue dye. The reusability studies showed promising values as not much change in degradation efficiency and rate was observed. The reduction in the degradation rate was less than 5% between the first cycle and the third cycle. *Moringa oliefera* leaf extract was used to prepare iron nanoparticles for fluoride removal by Silveira *et al.* (2018). The regeneration was done by washing the adsorbent with 20% ethanol. The results showed little reduction in adsorption efficiency from 80.94 to 80.44% after the first wash. The decrease in later cycles was up to 75% and it was possible to reuse it three times. Pan *et al.* (2019) synthesized nZVI using red peanut skin extract for the removal of Cr(VI). Hydrochloric acid (16 M) was used as a regenerant and caused desorption of 70.2% Cr(VI). The removal efficiency of desorbed iron nanoparticles decreased significantly to 59.9% in the second cycle from complete removal in the first cycle. Ahmad *et al.* (2020) used date palm waste to synthesize nZVI for MB removal. The regeneration of nZVI was done using HCl (0.1 M). The removal efficiency decreased to 29.78% after four cycles of regeneration, while it was more than 80% in the first cycle.

6. SUMMARY AND FUTURE RESEARCH NEEDS

While the potential of chemically synthesized nZVI particles has been known for their efficiency in removing different classes of pollutants from water, their large-scale commercial application is limited due to several drawbacks such as high cost of manufacturing, usage of toxic chemicals, and contamination from precursor chemicals. This has resulted in studies on the development of plant-based nZVI, in recent years. As described in this paper, plant-based nZVI has shown improved material characteristics resulting in increased adsorption capacity for removing a variety of contaminants, such as dyes, heavy metals, nutrients and trace organic pollutants. Furthermore, plant-based nZVI particles have shown much less aggregation compared to chemically synthesized particles, resulting in more colloidal stability in solutions.

The studies show the use of different plant parts by researchers for the synthesis of nZVI, resulting in varied characteristics for the nZVI formed. The characteristics play an important role in the usefulness and efficiency of the material synthesized. Efforts should be made to identify the best plant materials suitable for the synthesis, based on local conditions. Plant-based synthesis using plants with high polyphenol and flavonoid contents should be attempted. Utilizing abundantly available weed plants for nZVI synthesis would be a sustainable approach. This approach would help to reduce waste and pollution, while simultaneously providing cost-effective and eco-friendly solutions for wastewater treatment. Functional groups responsible for the reduction of Fe^{+3} and their presence in synthesized nZVI should be correlated by conducting suitably detailed chemical analyses of plant extracts and nZVI. This can help in selecting the best plant parts for synthesizing nZVI and in optimizing the synthesis procedure. Furthermore, various chemical groups in plants have different reducing capacities and it is necessary to ensure uniformity in the synthesized nanoparticles. Thus, more studies should be conducted to characterize synthesized nZVI.

Most of the studies reported in the literature utilized small-scale laboratory batch tests under ideal conditions. More tests should be conducted to evaluate the performance of the medium in the presence of competing and interfering ions and compounds. A comparative long-term evaluation of the chemically synthesized and plant-based nanoparticles should be conducted on a large scale using real wastewater or natural water. This can reveal the true potential of plant-based nZVI.

Increasing the reusability of plant-based nZVI would not only reduce sludge production, but also make the process cost-effective. A few studies have shown that plant-based nZVI can be regenerated. More research should be conducted on different methods of regenerating the spent nZVI particles, such as solvent treatment and surface modification, and on evaluating their effectiveness in restoring the effectiveness of the original nZVI.

Several innovative applications of nZVI have been suggested recently, and several classes of pollutants have been shown to be effectively removed by plant-based nZVI particles. Efforts should be made to optimize the process parameters. Very few studies have been reported on the use of these particles for removing/inactivating pathogenic organisms from water, and more studies should be conducted on this aspect because nZVI can potentially be used as a medium for small-scale/household drinking water treatment due to its proven ability to remove various classes of chemical contaminants from water.

In summary, continued research on plant-based nZVI particles to fully understand their potential in wastewater treatment, especially for the removal of a wider variety of pollutants, and for improving sustainability and reducing the cost and environmental impact of the process, is necessary.

DATA AVAILABILITY STATEMENT

All relevant data are included in the paper or its Supplementary Information.

CONFLICT OF INTEREST

The authors declare there is no conflict.

REFERENCES

Abdelfatah, A. M., Fawzy, M., El-Khouly, M. E. & Eltaweil, A. S. 2021a Efficient adsorptive removal of tetracycline from aqueous solution using phytosynthesized nano-zero valent iron. *Journal of Saudi Chemical Society* **25** (12). https://doi.org/10.1016/j.jscs.2021.101365.

Abdelfatah, A. M., Fawzy, M., Eltaweil, A. S. & El-Khouly, M. E. 2021b Green synthesis of nano-zero-valent iron using Ricinus communis seeds extract: Characterization and application in the treatment of methylene blue-polluted water. *ACS Omega* **6** (39), 25397–25411. https://doi.org/10.1021/acsomega.1c03355.

Abd El-Monaem, E. M., Omer, A. M., El-Subruiti, G. M., Mohy-Eldin, M. S. & Eltaweil, A. S. 2022 Zero-valent iron supported-lemon derived biochar for ultra-fast adsorption of methylene blue. *Biomass Conversion and Biorefinery*. https://doi.org/10.1007/s13399-022-02362-y.

Abell, J. M., Özkundakci, D., Hamilton, D. P. & Reeves, P. 2022 Restoring shallow lakes impaired by eutrophication: Approaches, outcomes, and challenges. *Critical Reviews in Environmental Science and Technology* **52** (7), 1199–1246. https://doi.org/10.1080/10643389.2020.1854564.

Abida, O., Van der Graaf, F. & Li, L. Y. 2022 Exploratory study of removing nutrients from aqueous environments employing a green synthesised nano zero-valent iron. *Environmental Technology (United Kingdom)* **43** (13), 2017–2032. https://doi.org/10.1080/09593330.2020.1864480.

Adusei-Gyamfi, J. & Acha, V. 2016 Carriers for nano zerovalent iron (nZVI): Synthesis, application and efficiency. *RSC Advances* **6** (93), 91025–91044. https://doi.org/10.1039/c6ra16657a.

Ahmad, M., Akanji, M. A., Usman, A. R. A., Al-Farraj, A. S. F., Tsang, Y. F. & Al-Wabel, M. I. 2020 Turning date palm waste into carbon nanodots and nano zerovalent iron composites for excellent removal of methylthioninium chloride from water. *Scientific Reports* **10** (1). https://doi.org/10.1038/s41598-020-73097-x.

Aksu Demirezen, D., Yıldız, Y. Ş. & Demirezen Yılmaz, D. 2019 Amoxicillin degradation using green synthesized iron oxide nanoparticles: kinetics and mechanism analysis. *Environmental Nanotechnology, Monitoring and Management* **11**. https://doi.org/10.1016/j.enmm.2019.100219.

Alexander, J. T., Hai, F. I. & Al-aboud, T. M. 2012 Chemical coagulation-based processes for trace organic contaminant removal: Current state and future potential. *Journal of Environmental Management* **111**, 195–207. https://doi.org/10.1016/j.jenvman.2012.07.023.

Ali, H., Khan, E. & Ilahi, I. 2019 Environmental chemistry and ecotoxicology of hazardous heavy metals: Environmental persistence, toxicity, and bioaccumulation. *Journal of Chemistry* **2019**. https://doi.org/10.1155/2019/6730305.

Angaru, G. K. R., Lingamdinne, L. P., Choi, Y. L., Koduru, J. R., Yang, J. K. & Chang, Y. Y. 2021 Encapsulated zerovalent iron/nickel-fly ash zeolite foam for treating industrial wastewater contaminated by heavy metals. *Materials Today Chemistry* **22**. https://doi.org/10.1016/j.mtchem.2021.100577.

Arshadi, M., Abdolmaleki, M. K., Mousavinia, F., Foroughifard, S. & Karimzadeh, A. 2017 Nano modification of NZVI with an aquatic plant Azolla filiculoides to remove Pb(II) and Hg(II) from water: Aging time and mechanism study. *Journal of Colloid and Interface Science* **486**, 296–308. https://doi.org/10.1016/j.jcis.2016.10.002.

Badmus, K. O., Coetsee-Hugo, E., Swart, H. & Petrik, L. 2018 Synthesis and characterisation of stable and efficient nano zero valent iron. *Environmental Science and Pollution Research* **25** (24), 23667–23684. https://doi.org/10.1007/s11356-018-2119-7.

Bao, Y. & Zhang, G. 2012 Study of adsorption characteristics of methylene blue onto activated carbon made by salix psammophila. *Energy Procedia* **16** (B), 1141–1146. https://doi.org/10.1016/j.egypro.2012.01.182.

Benkhaya, S., Harfi, S. E. & Harfi, A. E. 2017 Classifications, properties and applications of textile dyes: A review. *Applied Journal of Environmental Engineering Science* **3**, 311–320.

Bharti, B., Kumar, R., Kumar, H., Li, H., Zha, X. & Ouyang, F. 2021 Advanced applications and current status of green nanotechnology in the environmental industry. In: *Green Functionalized Nanomaterials for Environmental Applications*. pp. 303–340. https://doi.org/10.1016/B978-0-12-823137-1.00012-9.

Bhatti, H. N., Iram, Z., Iqbal, M., Nisar, J. & Khan, M. I. 2020 Facile synthesis of zero valent iron and photocatalytic application for the degradation of dyes. *Materials Research Express* **7** (1). https://doi.org/10.1088/2053-1591/ab66a0.

Cao, D., Jin, X., Gan, L., Wang, T. & Chen, Z. 2016 Removal of phosphate using iron oxide nanoparticles synthesized by eucalyptus leaf extract in the presence of CTAB surfactant. *Chemosphere* **159**, 23–31. https://doi.org/10.1016/j.chemosphere.2016.05.080.

Conde-Cid, M., Paíga, P., Moreira, M. M., Albergaria, J. T., Álvarez-Rodríguez, E., Arias-Estévez, M. & Delerue-Matos, C. 2021 Sulfadiazine removal using green zero-valent iron nanoparticles: A low-cost and eco-friendly alternative technology for water remediation. *Environmental Research* **198**. https://doi.org/10.1016/j.envres.2020.110451.

Desalegn, B., Megharaj, M., Chen, Z. & Naidu, R. 2019 Green synthesis of zero valent iron nanoparticle using mango peel extract and surface characterization using XPS and GC-MS. *Heliyon* **5** (5), e01750.

Devatha, C. P., Thalla, A. K. & Katte, S. Y. 2016 Green synthesis of iron nanoparticles using different leaf extracts for treatment of domestic waste water. *Journal of Cleaner Production* **139**, 1425–1435. https://doi.org/10.1016/j.jclepro.2016.09.019.

Dikshit, P. K., Kumar, J., Das, A. K., Sadhu, S., Sharma, S., Singh, S., Gupta, P. K. & Kim, B. S. 2021 Green synthesis of metallic nanoparticles: Applications and limitations. *Catalysts* **11** (8). https://doi.org/10.3390/catal11080902.

Donadelli, J. A., Carlos, L., Arques, A. & García Einschlag, F. S. 2018 Kinetic and mechanistic analysis of azo dyes decolorization by ZVI-assisted fenton systems: pH-dependent shift in the contributions of reductive and oxidative transformation pathways. *Applied Catalysis B: Environmental* **231**, 51–61. https://doi.org/10.1016/j.apcatb.2018.02.057.

Du, C., Chen, H., Gao, W., Sun, W., Peng, L. & Xu, N. 2023 Green synthesis of nano-zero valence iron with green tea and it's implication in lead removal. *Bulletin of Environmental Contamination and Toxicology* **110** (1). https://doi.org/10.1007/s00128-022-03649-6.

Ebrahiminezhad, A., Zare-Hoseinabadi, A., Berenjian, A. & Ghasemi, Y. 2017 Green synthesis and characterization of zero-valent iron nanoparticles using stinging nettle (Urtica dioica) leaf extract. *Green Processing and Synthesis* **6** (5), 469–475. https://doi.org/10.1515/gps-2016-0133.

Ebrahiminezhad, A., Taghizadeh, S., Ghasemi, Y. & Berenjian, A. 2018 Green synthesized nanoclusters of ultra-small zero valent iron nanoparticles as a novel dye removing material. *Science of the Total Environment* **621**, 1527–1532. https://doi.org/10.1016/j.scitotenv.2017.10.076.

Eljamal, R., Eljamal, O., Maamoun, I., Yilmaz, G. & Sugihara, Y. 2020 Enhancing the characteristics and reactivity of nZVI: Polymers effect and mechanisms. *Journal of Molecular Liquids* **315**. https://doi.org/10.1016/j.molliq.2020.113714.

Fatimah, I., Zunita Pratiwi, E. & Prio Wicaksono, W. 2020 Synthesis of magnetic nanoparticles using Parkia speciosa Hassk pod extract and photocatalytic activity for Bromophenol blue degradation. *Egyptian Journal of Aquatic Research* **46** (1), 35–40. https://doi.org/10.1016/j.ejar.2020.01.001.

Fazlzadeh, M., Rahmani, K., Zarei, A., Abdoallahzadeh, H., Nasiri, F. & Khosravi, R. 2017 A novel green synthesis of zero valent iron nanoparticles (NZVI) using three plant extracts and their efficient application for removal of Cr(VI) from aqueous solutions. *Advanced Powder Technology* **28** (1), 122–130. https://doi.org/10.1016/j.apt.2016.09.003.

Francy, N., Shanthakumar, S., Chiampo, F. & Sekhar, Y. R. 2020 Remediation of lead and nickel contaminated soil using nanoscale zero-valent iron (Nzvi) particles synthesized using green leaves: First results. *Processes* **8** (11), 1–12. https://doi.org/10.3390/pr8111453.

Gautam, A., Rawat, S., Verma, L., Singh, J., Sikarwar, S., Yadav, B. C. & Kalamdhad, A. S. 2018 Green synthesis of iron nanoparticle from extract of waste tea: An application for phenol red removal from aqueous solution. *Environmental Nanotechnology, Monitoring and Management* **10**, 377–387. https://doi.org/10.1016/j.enmm.2018.08.003.

Govarthanan, M., Jeon, C. H., Jeon, Y. H., Kwon, J. H., Bae, H. & Kim, W. 2020 Non-toxic nano approach for wastewater treatment using Chlorella vulgaris exopolysaccharides immobilized in iron-magnetic nanoparticles. *International Journal of Biological Macromolecules* **162**, 1241–1249. https://doi.org/10.1016/j.ijbiomac.2020.06.227.

Hamzezadeh, A., Fazlzadeh, M., Rahmani, K. & Poureshgh, Y. 2021 A novel green synthesis of zero valent iron nanoparticles (nZVI) using walnut green skin: Characterisation, catalytic degradation and toxicity studies. *International Journal of Environmental Analytical Chemistry*, 1–17. https://doi.org/10.1080/03067319.2021.1957463.

Hassan, M., Naidu, R., Du, J., Liu, Y. & Qi, F. 2020 Critical review of magnetic biosorbents: Their preparation, application, and regeneration for wastewater treatment. *Science of the Total Environment* **702**. https://doi.org/10.1016/j.scitotenv.2019.134893.

Huang, L., Weng, X., Chen, Z., Megharaj, M. & Naidu, R. 2014 Green synthesis of iron nanoparticles by various tea extracts: Comparative study of the reactivity. *Spectrochimica Acta – Part A: Molecular and Biomolecular Spectroscopy* **130**, 295–301. https://doi.org/10.1016/j.saa.2014.04.037.

Huang, L., Luo, F., Chen, Z., Megharaj, M. & Naidu, R. 2015 Green synthesized conditions impacting on the reactivity of Fe NPs for the degradation of malachite green. *Spectrochimica Acta – Part A: Molecular and Biomolecular Spectroscopy* **137**, 154–159. https://doi.org/10.1016/j.saa.2014.08.116.

Huston, M., Debella, M., Dibella, M. & Gupta, A. 2021 Green synthesis of nanomaterials. *Nanomaterials* **11** (8). https://doi.org/10.3390/nano11082130.

Jain, R., Mendiratta, S., Kumar, L. & Srivastava, A. 2021 Green synthesis of iron nanoparticles using Artocarpus heterophyllus peel extract and their application as a heterogeneous Fenton-like catalyst for the degradation of Fuchsin Basic dye. *Current Research in Green and Sustainable Chemistry* **4**. https://doi.org/10.1016/j.crgsc.2021.100086.

Jamkhande, P. G., Ghule, N. W., Bamer, A. H. & Kalaskar, M. G. 2019 Metal nanoparticles synthesis: An overview on methods of preparation, advantages and disadvantages, and applications. *Journal of Drug Delivery Science and Technology* **53**. https://doi.org/10.1016/j.jddst.2019.101174.

Jeyasundari, J., Shanmuga Praba, P., Brightson, Y., Jacob, A., Vasantha, V. S. & Shanmugaiah, V. 2017 Chemical science review and letters green synthesis and characterization of zero valent iron nanoparticles from the leaf extract of Psidium guajava plant and their antibacterial activity. *Chemical Science Review and Letters* **6** (22), 1244–1252.

Jha, A. K. & Chakraborty, S. 2020 Photocatalytic degradation of Congo Red under UV irradiation by zero valent iron nano particles (nZVI) synthesized using Shorea robusta (Sal) leaf extract. *Water Science and Technology* **82** (11), 2491–2502. https://doi.org/10.2166/wst.2020.517.

Jha, A. K. & Chakraborty, S. 2023 Photocatalytic degradation of tetracycline and ciprofloxacin antibiotic residues in aqueous phase by biosynthesized nZVI using Sal (Shorea robusta) leaf extract. *Journal of Water Supply: Research and Technology-Aqua* **72** (3), 230–245. https://doi.org/10.2166/aqua.2023.113.

Jiang, Q., Song, X., Liu, J., Shao, Y. & Feng, Y. 2019 Enhanced nutrients enrichment and removal from eutrophic water using a self-sustaining in situ photomicrobial nutrients recovery cell (PNRC). *Water Research* **167**. https://doi.org/10.1016/j.watres.2019.115097.

Kadhom, M., Albayati, N., Alalwan, H. & Al-Furaiji, M. 2020 Removal of dyes by agricultural waste. *Sustainable Chemistry and Pharmacy* **16**. https://doi.org/10.1016/j.scp.2020.100259.

Kalra, A. & Gupta, A. 2019 Recent advances in decolourization of dyes using iron nanoparticles: A mini review. *Materials Today: Proceedings* **36**, 689–696. https://doi.org/10.1016/j.matpr.2020.04.677.

Kamath, V., Chandra, P. & Jeppu, G. P. 2020 Comparative study of using five different leaf extracts in the green synthesis of iron oxide nanoparticles for removal of arsenic from water. *International Journal of Phytoremediation* **22** (12), 1278–1294. https://doi.org/10.1080/15226514.2020.1765139.

Karam, A., Zaher, K. & Mahmoud, A. S. 2020 Comparative studies of using nano zerovalent iron, activated carbon, and green synthesized nano zerovalent iron for textile wastewater colour removal using artificial intelligence, regression analysis, adsorption isotherm, and kinetic studies. *Air, Soil and Water Research* **13**. https://doi.org/10.1177/1178622120908273.

Khandel, P., Yadaw, R. K., Soni, D. K., Kanwar, L. & Shahi, S. K. 2018 Biogenesis of metal nanoparticles and their pharmacological applications: Present status and application prospects. *Journal of Nanostructure in Chemistry* **8** (3), 217–254. https://doi.org/10.1007/s40097-018-0267-4.

Khashij, M., Dalvand, A., Mehralian, M., Ebrahimi, A. A. & Khosravi, R. 2020 Removal of reactive black 5 dye using zero valent iron nanoparticles produced by a novel green synthesis method. *Pigment and Resin Technology* **49** (3), 215–221. https://doi.org/10.1108/PRT-10-2019-0092.

Khunjan, U. & Kasikamphaiboon, P. 2021 Green synthesis of kaolin-supported nanoscale zero-valent iron using Ruellia tuberosa leaf extract for effective decolorization of azo dye reactive black 5. *Arabian Journal for Science and Engineering* **46** (1), 383–394. https://doi.org/10.1007/s13369-020-04831-w.

Kończak, M. & Huber, M. 2022 Application of the engineered sewage sludge-derived biochar to minimize water eutrophication by removal of ammonium and phosphate ions from water. *Journal of Cleaner Production* **331**. https://doi.org/10.1016/j.jclepro.2021.129994.

Kozma, G., Rónavári, A., Kónya, Z. & Kukovecz, Á. 2016 Environmentally benign synthesis methods of zero-valent iron nanoparticles. *ACS Sustainable Chemistry and Engineering* **4** (1), 291–297. https://doi.org/10.1021/acssuschemeng.5b01185.

Latif, A., Sheng, D., Sun, K., Si, Y., Azeem, M., Abbas, A. & Bilal, M. 2020 Remediation of heavy metals polluted environment using Fe-based nanoparticles: Mechanisms, influencing factors, and environmental implications. *Environmental Pollution* **264**. https://doi.org/10.1016/j.envpol.2020.114728.

Leili, M., Fazlzadeh, M. & Bhatnagar, A. 2018 Green synthesis of nano-zero-valent iron from Nettle and Thyme leaf extracts and their application for the removal of cephalexin antibiotic from aqueous solutions. *Environmental Technology (United Kingdom)* **39** (9), 1158–1172. https://doi.org/10.1080/09593330.2017.1323956.

Li, Q., Cai, T., Huang, Y., Xia, X., Cole, S. P. C. & Cai, Y. 2017a A review of the structure, preparation, and application of NLCs, PNPs, and PLNs. *Nanomaterials* **7** (6). https://doi.org/10.3390/nano7060122.

Li, S., Wang, W., Liang, F. & Zhang, W. X. 2017b Heavy metal removal using nanoscale zero-valent iron (nZVI): Theory and application. *Journal of Hazardous Materials* **322**, 163–171. https://doi.org/10.1016/j.jhazmat.2016.01.032.

Li, Q., Chen, Z., Wang, H., Yang, H., Wen, T., Wang, S., Hu, B. & Wang, X. 2021 Removal of organic compounds by nanoscale zero-valent iron and its composites. *Science of the Total Environment* **792**. https://doi.org/10.1016/j.scitotenv.2021.148546.

Li, X., Jie, B., Lin, H., Deng, Z., Qian, J., Yang, Y. & Zhang, X. 2022 Application of sulfate radicals-based advanced oxidation technology in degradation of trace organic contaminants (TrOCs): Recent advances and prospects. *Journal of Environmental Management* **308**. https://doi.org/10.1016/j.jenvman.2022.114664.

Li, X., Wang, C., Chen, X., Li, D. & Jin, Q. 2023 Enhanced oxidation and removal of As(III) from water using biomass-derived porous carbon-supported nZVI with high iron utilization and fast adsorption. *Journal of Environmental Chemical Engineering* **11** (1). https://doi.org/10.1016/j.jece.2022.109038.

Lim, S. N., Ng, W. M., Lim, J. K. & Che, H. X. 2018 Performance of mulberry leaves mediated green synthesis zero-valent iron nanoparticles in dye removal. *International Journal of Engineering & Technology* **7** (3), 113.

Lin, Z., Weng, X., Owens, G. & Chen, Z. 2020 Simultaneous removal of Pb(II) and rifampicin from wastewater by iron nanoparticles synthesized by a tea extract. *Journal of Cleaner Production* **242**. https://doi.org/10.1016/j.jclepro.2019.118476.

Lin, J., Xue, C., Guo, S., Owens, G. & Chen, Z. 2021 Effects of green synthesized and commercial nZVI on crystal violet degradation by Burkholderia vietnamiensis c09v: Dose-dependent toxicity and biocompatibility. *Chemosphere* **279**. https://doi.org/10.1016/j.chemosphere.2021.130612.

Liu, A., Liu, J., Han, J. & Zhang, W. X. 2017 Evolution of nanoscale zero-valent iron (nZVI) in water: Microscopic and spectroscopic evidence on the formation of nano- and micro-structured iron oxides. *Journal of Hazardous Materials* **322**, 129–135. https://doi.org/10.1016/j.jhazmat.2015.12.070.

Lu, F. & Astruc, D. 2020 Nanocatalysts and other nanomaterials for water remediation from organic pollutants. *Coordination Chemistry Reviews* **408**. https://doi.org/10.1016/j.ccr.2020.213180.

Machado, S., Grosso, J. P., Nouws, H. P. A., Albergaria, J. T. & Delerue-Matos, C. 2014 Utilization of food industry wastes for the production of zero-valent iron nanoparticles. *Science of the Total Environment* **496**, 233–240. https://doi.org/10.1016/j.scitotenv.2014.07.058.

Machado, S., Pacheco, J. G., Nouws, H. P. A., Albergaria, J. T. & Delerue-Matos, C. 2015 Characterization of green zero-valent iron nanoparticles produced with tree leaf extracts. *Science of the Total Environment* **533**, 76–81. https://doi.org/10.1016/j.scitotenv.2015.06.091.

Mahajan, G., Kaur, M. & Gupta, R. 2021 Green functionalized nanomaterials: Fundamentals and future opportunities. In: *Green Functionalized Nanomaterials for Environmental Applications*. pp. 21–41. https://doi.org/10.1016/B978-0-12-823137-1.00003-8.

Makarov, V. V., Love, A. J., Sinitsyna, O. V., Makarova, S. S., Yaminsky, I. V., Taliansky, M. E. & Kalinina, N. O. 2014 'Green' nanotechnologies: Synthesis of metal nanoparticles using plants. *Acta Naturae* **6** (1(20)), 35–44.

Manquián-Cerda, K., Cruces, E., Angélica Rubio, M., Reyes, C. & Arancibia-Miranda, N. 2017 Preparation of nanoscale iron (oxide, oxyhydroxides and zero-valent) particles derived from blueberries: Reactivity, characterization and removal mechanism of arsenate. *Ecotoxicology and Environmental Safety* **145**, 69–77. https://doi.org/10.1016/j.ecoenv.2017.07.004.

Mu, Y., Jia, F., Ai, Z. & Zhang, L. 2017 Iron oxide shell mediated environmental remediation properties of nano zero-valent iron. *Environmental Science: Nano* **4** (1), 27–45. https://doi.org/10.1039/C6EN00398B.

Naseem, T. & Farrukh, M. A. 2015 Antibacterial activity of green synthesis of iron nanoparticles using Lawsonia inermis and Gardenia jasminoides leaves extract. *Journal of Chemistry* **2015**. https://doi.org/10.1155/2015/912342.

Nasiri, J., Motamedi, E., Naghavi, M. R. & Ghafoori, M. 2019 Removal of crystal violet from water using *B*-cyclodextrin functionalized biogenic zero-valent iron nanoadsorbents synthesized via aqueous root extracts of Ferula persica. *Journal of Hazardous Materials* **367**, 325–338. https://doi.org/10.1016/j.jhazmat.2018.12.079.

Nasrollahzadeh, M., Sajjadi, M., Iravani, S. & Varma, R. S. 2021 Green-synthesized nanocatalysts and nanomaterials for water treatment: Current challenges and future perspectives. *Journal of Hazardous Materials* **401**. https://doi.org/10.1016/j.jhazmat.2020.123401.

Pan, Z., Lin, Y., Sarkar, B., Owens, G. & Chen, Z. 2019 Green synthesis of iron nanoparticles using red peanut skin extract: Synthesis mechanism, characterization and effect of conditions on chromium removal. *Journal of Colloid and Interface Science* **558**, 106–114. https://doi.org/10.1016/j.jcis.2019.09.106.

Pandey, A., Shukla, P. & Srivastava, P. K. 2020 Remediation of dyes in water using green synthesized nanoparticles (NPs). *International Journal of Plant and Environment* **6** (1), 68–84. https://doi.org/10.18811/ijpen.v6i01.08.

Parlayıcı, Ş. & Pehlivan, E. 2019 Fast decolorization of cationic dyes by nano-scale zero valent iron immobilized in sycamore tree seed pod fibers: Kinetics and modelling study. *International Journal of Phytoremediation* **21** (11), 1130–1144. https://doi.org/10.1080/15226514.2019.1606786.

Pasinszki, T. & Krebsz, M. 2020 Synthesis and application of zero-valent iron nanoparticles in water treatment, environmental remediation, catalysis, and their biological effects. *Nanomaterials* **10** (5). https://doi.org/10.3390/nano10050917.

Pattanayak, M., Mohapatra, D. & Nayak, P. L. 2013 Green synthesis and characterization of zero valent iron nanoparticles from the leaf extract of syzygium aromaticum (clove). *Middle East Journal of Scientific Research* **18** (5), 623–626. https://doi.org/10.5829/idosi.mejsr.2013.18.5.11729.

Pattanayak, D. S., Pal, D., Thakur, C., Kumar, S. & Devnani, G. L. 2021 Bio-synthesis of iron nanoparticles for environmental remediation: Status till date. *Materials Today: Proceedings* **44**, 3150–3155. https://doi.org/10.1016/j.matpr.2021.02.821.

Poguberović, S. S., Krčmar, D. M., Maletić, S. P., Kónya, Z., Pilipović, D. D. T., Kerkez, D. V. & Rončević, S. D. 2016 Removal of As(III) and Cr(VI) from aqueous solutions using 'green' zero-valent iron nanoparticles produced by oak, mulberry and cherry leaf extracts. *Ecological Engineering* **90**, 42–49. https://doi.org/10.1016/j.ecoleng.2016.01.083.

Pourabadeh, A., Baharinikoo, L., Shojaei, S., Mehdizadeh, B., Davoodabadi Farahani, M. & Shojaei, S. 2020 Experimental design and modelling of removal of dyes using nano-zero-valent iron: A simultaneous model. *International Journal of Environmental Analytical Chemistry* **100** (15), 1707–1719. https://doi.org/10.1080/03067319.2019.1657855.

Pourali, P., Behzad, A., Ahmadfazeli, A., Mokhtari, S. A., Rashtbari, Y. & Poureshgh, Y. 2022 Dissociation of acid blue 113 dye from aqueous solutions using activated persulfate by zero iron nanoparticle from green synthesis: The optimization process with RSM-BBD model: Mineralization and reaction kinetic study. *Biomass Conversion and Biorefinery*. https://doi.org/10.1007/s13399-022-02942-y.

Prabhakar, R., Samadder, S. R. & Jyotsana 2017 Aquatic and terrestrial weed mediated synthesis of iron nanoparticles for possible application in wastewater remediation. *Journal of Cleaner Production* **168**, 1201–1210. https://doi.org/10.1016/j.jclepro.2017.09.063.

Priya, N., Kaur, K. & Sidhu, A. K. 2021 Green synthesis: An eco-friendly route for the synthesis of iron oxide nanoparticles. *Frontiers in Nanotechnology* **3**. https://doi.org/10.3389/fnano.2021.655062.

Quan, G., Kong, L., Lan, Y., Yan, J. & Gao, B. 2018 Removal of acid orange 7 by surfactant-modified iron nanoparticle supported on palygorskite: Reactivity and mechanism. *Applied Clay Science* **152**, 173–182. https://doi.org/10.1016/j.clay.2017.11.011.

Raman, C. D., Sellappa, K. & Mkandawire, M. 2021 Facile one step green synthesis of iron nanoparticles using grape leaves extract: Textile dye decolorization and wastewater treatment. *Water Science and Technology* **83** (9), 2242–2258. https://doi.org/10.2166/wst.2021.140.

Rana, A., Kumari, N., Tyagi, M. & Jagadevan, S. 2018 Leaf-extract mediated zero-valent iron for oxidation of arsenic (III): Preparation, characterization and kinetics. *Chemical Engineering Journal* **347**, 91–100. https://doi.org/10.1016/j.cej.2018.04.075.

Rashtbari, Y., Hazrati, S., Azari, A., Afshin, S., Fazlzadeh, M. & Vosoughi, M. 2020 A novel, eco-friendly and green synthesis of PPAC-ZnO and PPAC-nZVI nanocomposite using pomegranate peel: Cephalexin adsorption experiments, mechanisms, isotherms and kinetics. *Advanced Powder Technology* **31** (4), 1612–1623. https://doi.org/10.1016/j.apt.2020.02.001.

Sahu, N., Rawat, S., Singh, J., Karri, R. R., Lee, S., Choi, J. S. & Koduru, J. R. 2019 Process optimization and modeling of methylene blue adsorption using zero-valent iron nanoparticles synthesized from sweet lime pulp. *Applied Sciences (Switzerland)* **9** (23). https://doi.org/10.3390/app9235112.

Samadi, Z., Yaghmaeian, K., Mortazavi-Derazkola, S., Khosravi, R., Nabizadeh, R. & Alimohammadi, M. 2021 Facile green synthesis of zero-valent iron nanoparticles using barberry leaf extract (GnZVI@ BLE) for photocatalytic reduction of hexavalent chromium. *Bioorganic Chemistry* **114** (105051). https://doi.org/10.1016/j.bioorg.2021.105051.

Samuel, M. S., Selvarajan, E., Chidambaram, R., Patel, H. & Brindhadevi, K. 2021 Clean approach for chromium removal in aqueous environments and role of nanomaterials in bioremediation: Present research and future perspective. *Chemosphere* **284**. https://doi.org/10.1016/j.chemosphere.2021.131368.

Saravanan, A., Kumar, P. S., Karishma, S., Vo, D. V. N., Jeevanantham, S., Yaashikaa, P. R. & George, C. S. 2021 A review on biosynthesis of metal nanoparticles and its environmental applications. *Chemosphere* **264**. https://doi.org/10.1016/j.chemosphere.2020.128580.

Shad, S., Belinga-Desaunay-Nault, M. F. A., Sohail, Bashir, N. & Lynch, I. 2020 Removal of contaminants from canal water using microwave synthesized zero valent iron nanoparticles. *Environmental Science: Water Research and Technology* **6** (11), 3057–3065. https://doi.org/10.1039/d0ew00157k.

Shafey, A. M. E. 2020 Green synthesis of metal and metal oxide nanoparticles from plant leaf extracts and their applications: A review. *Green Processing and Synthesis* **9** (1), 304–339. https://doi.org/10.1515/gps-2020-0031.

Shahwan, T., Abu Sirriah, S., Nairat, M., Boyaci, E., Eroğlu, A. E., Scott, T. B. & Hallam, K. R. 2011 Green synthesis of iron nanoparticles and their application as a Fenton-like catalyst for the degradation of aqueous cationic and anionic dyes. *Chemical Engineering Journal* **172** (1), 258–266. https://doi.org/10.1016/j.cej.2011.05.103.

Shaibu, S. E., Adekola, F. A., Adegoke, H. I. & Ayanda, O. S. 2014 A comparative study of the adsorption of methylene blue onto synthesized nanoscale zero-valent iron-bamboo and manganese-bamboo composites. *Materials* **7** (6), 4493–4507. https://doi.org/10.3390/ma7064493.

Shanableh, A., Bhattacharjee, S. & Sadik, S. 2021 Evaluating iron-based nanoparticles for ciprofloxacin removal: Date seed extract as a biostabilizing and a bioreducing agent. *Journal of Water Process Engineering* **44**, 102419.

Sharma, D., Kanchi, S. & Bisetty, K. 2019 Biogenic synthesis of nanoparticles: A review. *Arabian Journal of Chemistry* **12** (8), 3576–3600. https://doi.org/10.1016/j.arabjc.2015.11.002.

Shi, Z., Fan, D., Johnson, R. L., Tratnyek, P. G., Nurmi, J. T., Wu, Y. & Williams, K. H. 2015 Methods for characterizing the fate and effects of nano zerovalent iron during groundwater remediation. *Journal of Contaminant Hydrology* **181**, 17–35. https://doi.org/10.1016/j.jconhyd.2015.03.004.

Shin, M. G., Choi, W., Park, S. J., Jeon, S., Hong, S. & Lee, J. H. 2022 Critical review and comprehensive analysis of trace organic compound (TOrC) removal with polyamide RO/NF membranes: Mechanisms and materials. *Chemical Engineering Journal* **427**. https://doi.org/10.1016/j.cej.2021.130957.

Silveira, C., Shimabuku, Q. L., Fernandes Silva, M. & Bergamasco, R. 2018 Iron-oxide nanoparticles by the green synthesis method using Moringa oleifera leaf extract for fluoride removal. *Environmental Technology (United Kingdom)* **39** (22), 2926–2936. https://doi.org/10.1080/09593330.2017.1369582.

Simseka, U. B., Turabika, M. & Treatment, W. 2017 Decolorization mechanisms of an anionic dye by using zero-valent iron nanoparticles: Application of response surface modelling for the optimization process. *Desalination and Water Treatment* **81**, 303–314.

Singh, A., Madhavi, B. & Nithin Sagar, M. N. 2021 An overview of green synthesis mediated metal nanoparticles preparation and its scale up opportunities. *Journal of Drug Delivery and Therapeutics* **11** (6), 304–314. https://doi.org/10.22270/jddt.v11i6.5082.

Speisky, H., Shahidi, F., Costa de Camargo, A. & Fuentes, J. 2022 Revisiting the oxidation of flavonoids: Loss, conservation or enhancement of their antioxidant properties. *Antioxidants* **11** (1), 133.

Sravanthi, K., Ayodhya, D. & Yadgiri Swamy, P. 2018 Green synthesis, characterization of biomaterial-supported zero-valent iron nanoparticles for contaminated water treatment. *Journal of Analytical Science and Technology* **9** (3), 1–11.

Stefaniuk, M., Oleszczuk, P. & Ok, Y. S. 2016 Review on nano zerovalent iron (nZVI): From synthesis to environmental applications. *Chemical Engineering Journal* **287**, 618–632. https://doi.org/10.1016/j.cej.2015.11.046.

Sunardi, Ashadi, Rahardjo, S. B. & Inayati 2017 Ecofriendly synthesis of nano zero valent iron from banana peel extract. *Journal of Physics: Conference Series* **795** (1), 012063. https://doi.org/10.1088/1742-6596/795/1/012063.

Tang, H., Wang, J., Zhang, S., Pang, H., Wang, X., Chen, Z., Li, M., Song, G., Qiu, M. & Yu, S. 2021 Recent advances in nanoscale zero-valent iron-based materials: Characteristics, environmental remediation and challenges. *Journal of Cleaner Production* **319**. https://doi.org/10.1016/j.jclepro.2021.128641.

Tarekegn, M. M., Hiruy, A. M. & Dekebo, A. H. 2021 Nano zero valent iron (nZVI) particles for the removal of heavy metals (Cd2 + , Cu2 + and Pb2+) from aqueous solutions. *RSC Advances* **11** (30), 18539–18551. https://doi.org/10.1039/d1ra01427g.

Tufail, A., Price, W. E. & Hai, F. I. 2020 A critical review on advanced oxidation processes for the removal of trace organic contaminants: A voyage from individual to integrated processes. *Chemosphere* **260**. https://doi.org/10.1016/j.chemosphere.2020.127460.

Venkatas, J., Daniels, A. & Singh, M. 2022 The potential of curcumin-capped nanoparticle synthesis in cancer therapy: A green synthesis approach. *Nanomaterials* **12** (18). https://doi.org/10.3390/nano12183201.

Vilando, A., Roque, E., Benitez, M. A., Diva, J. R. & Ragindin, J. E. 2019 Production of green nano zero-valent iron (G-nZVI) particles using polyphenol extracts of tawa-tawa (Euphorbia hirta linn) leaves and green tea (Camelia sinensis) leaves. *MATEC Web of Conferences* **268**, 05005. https://doi.org/10.1051/matecconf/201926805005.

Wang, T., Lin, J., Chen, Z., Megharaj, M. & Naidu, R. 2014 Green synthesized iron nanoparticles by green tea and eucalyptus leaves extracts used for removal of nitrate in aqueous solution. *Journal of Cleaner Production* **83**, 413–419. https://doi.org/10.1016/j.jclepro.2014.07.006.

Wei, Y., Fang, Z., Zheng, L., Tan, L. & Tsang, E. P. 2016 Green synthesis of Fe nanoparticles using Citrus maxima peels aqueous extracts. *Materials Letters* **185**, 384–386.

Weng, X., Jin, X., Lin, J., Naidu, R. & Chen, Z. 2016 Removal of mixed contaminants Cr(VI) and Cu(II) by green synthesized iron based nanoparticles. *Ecological Engineering* **97**, 32–39. https://doi.org/10.1016/j.ecoleng.2016.08.003.

Wu, H., Yin, J. J., Wamer, W. G., Zeng, M. & Lo, Y. M. 2014 Reactive oxygen species-related activities of nano-iron metal and nano-iron oxides. *Journal of Food and Drug Analysis* **22** (1), 86–94. https://doi.org/10.1016/j.jfda.2014.01.007.

Wu, Z., Su, X., Lin, Z., Owens, G. & Chen, Z. 2019 Mechanism of As(V) removal by green synthesized iron nanoparticles. *Journal of Hazardous Materials* **379**. https://doi.org/10.1016/j.jhazmat.2019.120811.

Xu, Q., Li, W., Ma, L., Cao, D., Owens, G. & Chen, Z. 2020 Simultaneous removal of ammonia and phosphate using green synthesized iron oxide nanoparticles dispersed onto zeolite. *Science of the Total Environment* **703**. https://doi.org/10.1016/j.scitotenv.2019.135002.

Yan, W., Ramos, M. A. V., Koel, B. E. & Zhang, W. X. 2012 As(III) sequestration by iron nanoparticles: Study of solid-phase redox transformations with X-ray photoelectron spectroscopy. *Journal of Physical Chemistry C* **116** (9), 5303–5311. https://doi.org/10.1021/jp208600n.

Yang, J., Wang, S., Xu, N., Ye, Z., Yang, H. & Huangfu, X. 2021 Synthesis of montmorillonite-supported nano-zero-valent iron via green tea extract: Enhanced transport and application for hexavalent chromium removal from water and soil. *Journal of Hazardous Materials* **419**. https://doi.org/10.1016/j.jhazmat.2021.126461.

Ying, S., Guan, Z., Ofoegbu, P. C., Clubb, P., Rico, C., He, F. & Hong, J. 2022 Green synthesis of nanoparticles: Current developments and limitations. *Environmental Technology and Innovation* **26**. https://doi.org/10.1016/j.eti.2022.102336.

Yusmartini, E. S., Setiabudidaya, D., Ridwan, R., Marsi & Faizal, 2015 Synthesis and characterization of zero-valent iron nanoparticles. *Advanced Materials Research* **1112**, 62–65. https://doi.org/10.4028/www.scientific.net/amr.1112.62.

Zhou, Y. & Li, X. 2022 Green synthesis of modified polyethylene packing supported tea polyphenols-NZVI for nitrate removal from wastewater: Characterization and mechanisms. *Science of the Total Environment* **806**. https://doi.org/10.1016/j.scitotenv.2021.150596.

Zhou, L., Li, Z., Yi, Y., Tsang, E. P. & Fang, Z. 2022 Increasing the electron selectivity of nanoscale zero-valent iron in environmental remediation: A review. *Journal of Hazardous Materials* **421**. https://doi.org/10.1016/j.jhazmat.2021.126709.

Zikalala, N., Matshetshe, K., Parani, S. & Oluwafemi, O. S. 2018 Biosynthesis protocols for colloidal metal oxide nanoparticles. *Nano-Structures and Nano-Objects* **16**, 288–299. https://doi.org/10.1016/j.nanoso.2018.07.010.

First received 4 April 2023; accepted in revised form 15 August 2023. Available online 25 August 2023